Statistical analysis of particle trajectories in living cells

Vincent Briane, Charles Kervrann, Myriam Vimond

STATISTICAL ANALYSIS OF PARTICLE TRAJECTORIES IN LIVING CELLS

Vincent Briane,[1,2] Charles Kervrann,[1,*] and Myriam Vimond[2]
[1]Inria Rennes, Serpico Project Team, Campus Universitaire de Beaulieu, 35042 Rennes Cedex, France [2]CREST, Ensai, Université Bretagne Loire, Rue Blaise Pascal, 35172 Bruz, France

Recent advances in molecular biology and fluorescence microscopy imaging have made possible the inference of the dynamics of molecules in living cells. Such inference allows us to understand and determine the organization and function of the cell. The trajectories of particles (e.g., biomolecules) in living cells, computed with the help of object tracking methods, can be modeled with diffusion processes. Three types of diffusion are considered:(i) free diffusion, (ii) subdiffusion, and (iii) superdiffusion. The mean-square displacement (MSD) is generally used to discriminate the three types of particle dynamics. We propose here a nonparametric three-decision test as an alternative to the MSD method. The rejection of the null hypothesis, i.e., free diffusion, is accompanied by claims of the direction of the alternative (subdiffusion or superdiffusion). We study the asymptotic behavior of the test statistic under the null hypothesis and under parametric alternatives which are currently considered in the biophysics literature. In addition, we adapt the multiple-testing procedure of Benjamini and Hochberg to fit with the three-decision-test setting, in order to apply the test procedure to a collection of independent trajectories. The performance of our procedure is much better than the MSD method as confirmed by Monte Carlo experiments. The method is demonstrated on real data sets corresponding to protein dynamics observed in fluorescence microscopy.

I. INTRODUCTION

The dynamics of proteins determines the organization and function of the cell (see [1], Chap. 9). It is now established that intracellular trafficking is oriented and that the local dynamics of proteins obeys biophysical laws. Over the past few years, a number of stochastic mathematical models have been proposed in order to describe intracellular trafficking, where molecules are transported to their destinations via free diffusion (or Brownian motion), subdiffusion (diffusion in a closed domain or in an open but crowded area), and superdiffusion representing active transport along the cytoskeleton networks (e.g., microtubules, actin filaments, and intermediate filaments), assisted by molecular motors. Accordingly, the study of diffusion and stochastic dynamics has known a growing interest in biomathematics, biophysics, and cell biology, especially with the popularization of fluorescence dynamical microscopy accompanied by statistical object tracking methods [2]. Biological imaging has undergone a revolution in the development of new microscopy techniques that allow visualization of tissues, cells, proteins, and macromolecular structures at all levels of resolution, physiological states, chemical composition, and dynamics. Due to recent advances in optics, digital sensors, and labeling probes (e.g., colored fluorescent protein), one can now visualize subcellular components and organelles at the scale of several hundreds of nanometers to a few dozens of nanometers. All the technological advances in microscopy have created new issues and challenges in the statistical analysis of particle trajectories.

Actually, inference on the modes of mobility of molecules is central in cell biology since it reflects interactions with the internal structures of the cell. In this paper we will focus on the exocytosis mechanism and the transport of small vesicles from the interior of the cell towards the extracellular medium. As an other example, Lagache *et al.* [3] model the dynamics of a virus invading a cell to infer its mean arrival time to the cell nucleus where it replicates. In the model of Lagache *et al.* [3], the dynamic of the virus alternates between superdiffusion and Brownian motion. In this paper we are interested in the classification of individual intracellular particle trajectories into three modes of mobility: subdiffusion, free diffusion and superdiffusion (see Fig. 1). Usually, in the biophysics literature, the definition of these dynamics is related to the criterion of the mean-square displacement (MSD) (see, for example, [4]). Given a particle trajectory $(X_t)_{t>0}$, the MSD is defined as the function

$$\mathrm{MSD}(t) = \mathbb{E}(\|X_{t+t_0} - X_{t_0}\|^2), \tag{1}$$

where $\|\cdot\|$ is the Euclidean norm and $\mathbb{E}$ is the expectation of the probability space. If the MSD is linear [$\mathrm{MSD}(t) \propto t$], the trajectory is a free diffusion. In the biophysics literature [4,5], this kind of diffusion is associated with the Brownian motion (or Wiener process in mathematics). Kou [6] defines the physical Brownian motion via the Langevin equation with white noise, which is different from the biophysical Brownian motion. In this case we have $\mathrm{MSD}(t) \propto t$ for large t only. Bressloff [1] argues that both definitions of the Brownian motion can be used to model intracellular dynamics in the case where the particle evolves freely inside the cytosol or along the plasma membrane. We decided to pick the biophysical definition corresponding to the Wiener process in mathematics as Lysy *et al.* [7] did. If the MSD is sublinear, the trajectory is a subdiffusion (see [1], Chap. 7). Subdiffusion, which includes confined diffusion and anomalous subdiffusion, is appropriate to represent several biological scenarios. Confined or restricted

*Corresponding author: charles.kervrann@inria.fr

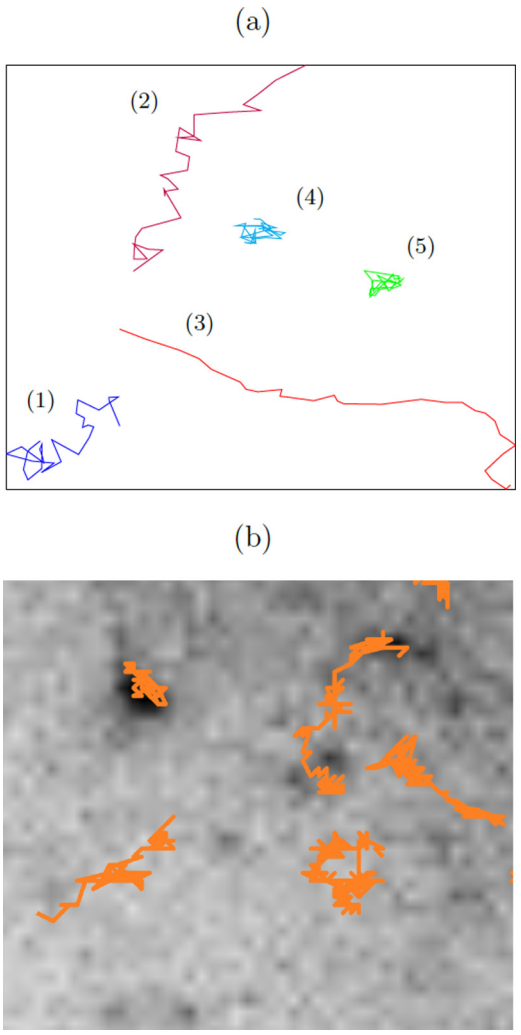

FIG. 1. Representative trajectories from (a) simulated data and (b) a Rab11a protein sequence in a single cell (courtesy of UMR No. 144, CNRS, Institut Curie, PICT IBiSA). For the simulated data in (a), trajectory (1) is Brownian, trajectory (2) is from Brownian motion with drift, trajectory (3) is from fractional Brownian motion (with the parameter $\mathfrak{h} > 1/2$), trajectory (4) is from an Ornstein-Uhlenbeck process, and trajectory (5) is from fractional Brownian motion ($\mathfrak{h} < 1/2$). The parameters of the processes are given in Table IV.

diffusion [8,9] is characteristic of trapped particles: The particle encounters a binding site and then it pauses for a while before dissociating and moving away. Anomalous subdiffusion includes particles which encounter dynamic or fixed obstacles [10,11] or particles slowed by the contrary current due to the viscoelastic properties of the cytoplasm. We note that anomalous subdiffusion is associated with a MSD function of the form $\mathrm{MSD}(t) \sim t^{\beta}$, with $\beta \in (0,1)$ [9]. In this paper we will not distinguish confined and anomalous subdiffusion and consider that both are subdiffusion. Meroz and Sokolov [12] present a wide range of models for subdiffusion including fractional Brownian motion and the Ornstein-Uhlenbeck process. The Ornstein-Uhlenbeck process is widely used for modeling subdiffusion as it is the solution of the overdamped Langevin equation [8,13]. Note that dedicated methods have been developed to distinguish fractional Brownian motion and continuous-time random walks [14]. In cell biology and biophysics, superdiffusion models the motion of molecular motors and their cargo: The motion is faster and in a specific direction. The main type of active intracellular transport involves molecular motors which carry particles (called, in this context, cargo) along microtubular filament tracks. Superdiffusion is associated with the case where the MSD function grows faster than the linear function (see [1], Chap. 7). Anomalous superdiffusion, the analog of anomalous subdiffusion, is associated with a MSD function of the form $\mathrm{MSD}(t) \sim t^{\beta}$, with $\beta > 1$ [9].

A. The problem

We observe the successive positions of a single particle $X_{t_0}, X_{t_1}, \ldots, X_{t_n}$ in the real plan at equispaced times, that is, $t_{i+1} - t_i = \Delta$. Our aim is to decide if the trajectory is a free diffusion, a subdiffusion or a superdiffusion. A popular statistic used to determine the motion model is the pathwise MSD. It is estimated at lag j by

$$\widehat{\mathrm{MSD}}(j\Delta) = \frac{1}{n-j+1} \sum_{k=0}^{n-j} \left\| X_{t_{k+j}} - X_{t_k} \right\|^2. \qquad (2)$$

Remark 1. The estimator of the MSD (2) is defined as a time average computed along a single trajectory. When we observe a population of trajectories which all undergo the same motion, one can estimate the theoretical MSD (1) with the ensemble-averaged estimator based on the observed displacements of all the trajectories [15]. We emphasize that both estimators, the time average and the ensemble average, aim to estimate the theoretical MSD (1). However, the time average (2) fails to converge to the theoretical MSD (1) if the underlying stochastic process is nonergodic [16–18]. In this paper, as our objective is to classify individually each trajectory, we must compare our method to a MSD method based on the time-averaged estimator (2).

The simplest rule to classify a trajectory with the MSD is based on the least-squares estimate of the slope β of the log-log plot of the MSD versus time [19]. Didier and Zhang [20] study the limiting distribution of the pathwise MSD according to the true value of β. Nevertheless, MSD has some limitations.

First, the variance increases with the time lag (see Fig. 2); only the first few points of the MSD may be used to estimate the slope. Moreover, the MSD variance is also severely affected at short time lags by dynamic localization error and motion blur. Michalet [15] details an iterative method, known as the optimal least-squares fit, for determining the optimal number of points to obtain the best fit to MSD in the presence of localization uncertainty.

In order to take account of the variance of the MSD estimate, several authors use a set of independent trajectories rather than single trajectories. These trajectories may have different lengths but are assumed to have the same kind of motion. For instance, Pisarev *et al.* [21] consider a weighted-least-squares estimate for β by estimating the variance of pathwise MSD. Their motion model selection is then based on the modified Akaike information criterion. Monnier *et al.* [22] propose a Bayesian approach to compute relative probabilities of an arbitrary set of motion models (free, confined, anomalous, or directed diffusion). In general, this averaging process can

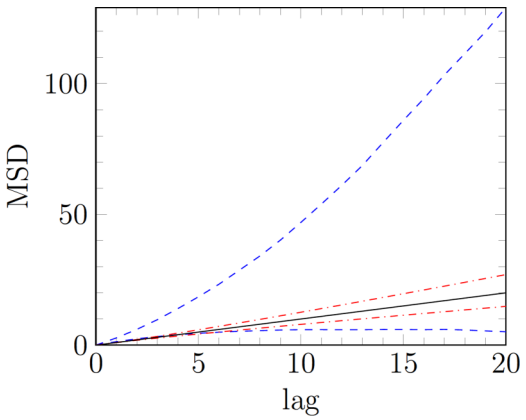

FIG. 2. Classification rule for motion modes from MSD. The solid line is the theoretical MSD of the standard Brownian motion. The dash-dotted lines are the bounds defined by [19]: $t \to t^{\beta}$, $\beta = 0.9$, and 1.1. If $\hat{\beta}$, the estimation of β, is such that $0.9 < \hat{\beta} < 1.1$ it is classified as Brownian motion. The dashed lines are the pointwise high-probability interval of 95% associated with the empirical MSD curve for a standard Brownian motion trajectory of length $n = 30$. The bounds of the interval are the 2.5% and 97.5% empirical quantiles of (2) and are computed by Monte Carlo simulation from 10 001 Brownian trajectories of size $n = 30$.

lead to oversimplification and misleading conclusions about the biological process [23].

Second, the MSD statistic is a summary statistic and does not suffice to characterize the dynamics of the trajectory. Gal *et al.* [23] present several other statistics which can be associated with MSD for trajectory analysis. Lund *et al.* [24] propose a decision tree for a selection motion model combining MSD, a Bayesian information criterion, and the radius of gyration [25]. Lysy *et al.* [7] present a likelihood-based inference as an alternative to MSD for the comparison between two models of subdiffusions: fractional Brownian motion and a generalized Langevin equation. They consider a Bayesian model to estimate the parameter of the diffusion and they use the Bayes factor to compare the models. Wagner *et al.* [26] combine different trajectory features including the radius of gyration, the fractional dimension, the kurtosis, and a ratio based on the MSD to classify the trajectories with random forests and then are able to classify individually each trajectory into four groups of diffusion. The algorithm comprises a training step in which simulated trajectories of each group of diffusion are used. The way the trajectories are simulated is of paramount importance as it influences very much the classification.

B. Our contribution

In this paper we propose a measure that circumvents some limitations of the MSD and is efficient for classifying single trajectories. Also, our method is not influenced by simulation choices, like the procedure of Wagner *et al.* [26], since we do not rely on simulations. Our procedure is a three-decision-test procedure [27]. The null hypothesis is that the observed trajectory is generated from a Brownian motion and the two distinct alternatives are subdiffusion and superdiffusion. The test statistic T_n is the standardized largest distance covered by the particle from its starting point. We interpret this measure as follows: (i) If the value of T_n is low, it means that the process stayed close to its initial position and the particle may be trapped in a small area or hindered by obstacles (subdiffusion), and (ii) if the value of T_n is high, the particle went far from its initial position and the particle may be driven by a motor in a certain direction (superdiffusion). In our model we restrict subdiffusion and superdiffusion to processes which are solutions of a stochastic differential equation. However, our procedure can be extended to others types of subdiffusion in principle (see Appendix B). Then we study the asymptotic behavior of our procedure under the null hypothesis and four parametric models illustrating superdiffusion and subdiffusion and which are commonly considered in the biophysics literature. As stated before, we will not distinguish confined and anomalous subdiffusion and consider that both are subdiffusion. The study of the behavior of the test statistic under all existing subdiffusion processes is beyond the scope of this paper. Ultimately, we derive a multiple-test procedure in order to simultaneously apply the test to a collection of independent trajectories which are tracked inside the same living cell. This procedure is an adaptation of the procedure of Benjamini and Hochberg [28]. It allows us to control the false discovery rate (FDR). Moreover, in the case of rejection of the null hypothesis, our multiple-test procedure is able to state for which alternative (subdiffusion or superdiffusion) we reject the null hypothesis.

The present paper is organized as follows. In Sec. II we describe the inference model and provide some examples of subdiffusion and superdiffusion. Our testing procedure is defined in Sec. III. In Sec. IV we derive a multiple-testing procedure for a collection of trajectories. We carry out a simulation study and illustrate the method on real data in Sec. V. We focus on the analysis of the Rab11a GTPase protein. This protein is involved in the trafficking of molecules from the endosomes located inside the cell to the cell plasma membrane. The data are computed from temporal sequences of total internal reflection fluorescence (TIRF) microscopy images depicting the last steps of exocytosis events observed in the region very close the plasma membrane [29]. Finally in Sec. VI we propose a modification of our test procedure to address two issues encountered in microscopy data namely, missing points and localization uncertainty. The proofs are postponed to Appendix A. The case of continuous-time random walk (CTRW) is discussed in Appendix B.

II. DIFFUSION MODELS FOR PARTICLE TRAJECTORY ANALYSIS

We observe the successive positions of a single particle in a two-dimensional space at times $t_0, t_1, \ldots, t_n$. We suppose that the lag time between two consecutive observations is a constant Δ. The observed trajectory of the particle is

$$\mathbb{X}_n = (X_{t_0}, X_{t_1}, \ldots, X_{t_n}),$$

where $X_{t_i} = (X^1_{t_i}, X^2_{t_i}) \in \mathbb{R}^2$ is the position of the particle at time $t_i = t_0 + i\Delta$, $i = 0, \ldots, n$. This discrete trajectory is generated by a stochastic process $(X_t)_{t_0 \leqslant t \leqslant t_n}$ with a continuous path and assumed to be solution of the stochastic differential equation (SDE)

$$dX^i_t = \mu_i(X^i_t)dt + \sigma dB^{\mathfrak{h},i}_t, \quad i = 1,2, \tag{3}$$

where $B_t^{\mathfrak{h},i}$ are unobserved, independent, one-dimensional fractional Brownian motions of unknown Hurst parameter $0 < \mathfrak{h} < 1$, $\sigma > 0$ is the unknown diffusion coefficient, and $(\mu_1(x_1),\mu_2(x_2)) : \mathbb{R}^2 \mapsto \mathbb{R}^2$ is the unknown drift term. We note that when $\mathfrak{h} = 1/2$ the SDE (3) is driven by Brownian motion. Then the solution of the SDE (3) is defined through Itô's theory of stochastic calculus developed for semimartingalelike Brownian motion [30]. When $\mathfrak{h} \neq 1/2$, the SDE (3) is driven by the fractional Brownian motion which has correlated increments. In this case, the definition of the solution of the SDE (3) is more involved (see [31], Chaps. 2 and 3).

Assumption 1. We assume that μ_i fulfills the linear growth hypothesis

$$|\mu_i(x)| \leqslant K(1 + |x|) \tag{4}$$

and the Lipschitz condition

$$|\mu_i(x) - \mu_i(y)| \leqslant M|x - y|. \tag{5}$$

We denote by $\mathcal{L}$ the set of functions verifying Assumption 1. Assumption 1 is sufficient to ensure that SDE (3) admits a strong solution (see [32] for the case $0 < \mathfrak{h} \leqslant 1/2$ and [31], Chap. 3, for the case $1/2 < \mathfrak{h} < 1$). For a given fractional Brownian motion, we say that X_t is a strong solution of the SDE (3) if X_t verifies (3), has continuous paths, and, at time t, depends only on X_{t_0} and on the trajectory of the fractional Brownian motion up to time t. In the following, $P_{\mathfrak{h},\mu,\sigma}$ denotes the measure induced by the stochastic process X_t solution of (3). This measure comprises all the finite-dimensional distributions of the process that is the distribution of the vectors $(X_{t_0},\ldots,X_{t_n}), n \in \mathbb{N}^*$, and $t_1 < \cdots < t_n$. We also note $\mathcal{P} = \{P_{\mathfrak{h},\mu,\sigma} : 0 < \mathfrak{h} < 1, \mu \in \mathcal{L}, \sigma > 0\}$, the set of solutions of the SDE (3).

Remark 2. In the following, we adopt the large-sample scheme to derive asymptotic properties of our procedure, that is, the interobservation time Δ remains fixed and the number of observations n tends to infinity. In the experimental context of microscopic sequences, Δ is the resolution of the microscopy device, while n is the number of frames during which we track the particle. Other schemes exist (see [33]) such as the high-frequency scheme for which Δ tends to zero while the duration of observation is fixed.

Heuristically, a SDE models the motion of a particle in a fluid submitted to a deterministic force due to the fluid and a random force due to random collisions with other particles. That is why we model efficiently the motion of intracellular particles with these processes. In Eq. (3), the velocity of the fluid is given by the drift μ, while the term $\sigma dB_t^{\mathfrak{h}}$ expresses the random component of the motion due to random collisions.

A. Free diffusion

Free diffusion or Brownian motion is the most popular process for describing particle motion suspended in a liquid [34]. It is particularly well suited for describing intracellular particle motion as the interior of the cell is mainly made of a fluid called the cytosol. Brownian motion allows dissolved macromolecules to be passively transported without any input of energy. In the SDE (3), it matches with the situation where the drift $\mu_i = 0$ and $\mathfrak{h} = 1/2$.

B. Subdiffusion

We present two models of subdiffusion which are solutions of the SDE (3). We give their MSD which is, by definition of subdiffusion, sublinear. The first subdiffusion is an example of confined diffusion, while the second is an anomalous subdiffusion. It corresponds to two distinct biological scenarios.

In the first scenario, the particle is attracted by an external force modeled by a potential well. We can then use the SDE (3) with a specific form for the drift $\mu_i(x) = -\nabla U_i(x)/\gamma_i$, where $-\nabla U_i$ is the external force of the fluid and γ_i is the frictional coefficient. For instance, we may consider the Ornstein-Uhlenbeck process

$$dX_t^i = -\lambda_i\big(X_t^i - \theta_i\big)dt + \sigma dB_t^{1/2,i}, \quad i = 1,2, \tag{6}$$

where $\lambda_i > 0$. Here the particle is assumed to be trapped in a single domain and the potential U is unimodal and is approximated by a polynomial of order 2: $U_i(x) = (1/2)k_i(x_i - \theta_i)^2$. The parameter $k_i = \lambda_i\gamma_i$ measures the strength of attraction of the potential (related to the potential depth), while $\theta = (\theta_1,\theta_2)$ is the equilibrium position of the particle. The Ornstein-Uhlenbeck process is a confined diffusion according to the MSD criterion since its MSD is sublinear,

$$\mathrm{MSD}(t) = \frac{2\sigma^2(1 - e^{-\lambda t})}{\lambda} \leqslant 2\sigma^2 t; \tag{7}$$

here it is written in the case $\lambda_i = \lambda$ for the sake of simplicity. A subdiffusion having this form of MSD is known as a confined diffusion [5,21,22].

Anomalous subdiffusion can occur for two main reasons. First, the particle can bind to an immobile trap that can generate long jump times [35]. In this situation, its motion can be modeled by a continuous-time random walk [9]. We study the performance of our test when subdiffusion is modeled by a continuous-time random walk in Appendix B. Hence we show that our procedure is still relevant even if the particle motion is not driven by the SDE (3). Second, the particle can be hindered by mobile or immobile obstacles as the interior environment of cells is crowded with solutes and macromolecules [36]. Thus, a popular model is the fractional Brownian motion [17], which corresponds to the case $0 < \mathfrak{h} < 1/2$ and $\mu_i = 0$ in (3),

$$dX_t^i = \sigma dB_t^{\mathfrak{h},i}, \quad i = 1,2. \tag{8}$$

Its MSD is given by

$$\mathrm{MSD}(t) = 2\sigma^2 t^{\beta} \leqslant 2\sigma^2 t, \tag{9}$$

with $\beta = 2\mathfrak{h} < 1$. As already mentioned in Sec. I, a subdiffusion having this form of MSD is known as an anomalous diffusion [5,9,21,22]. We note that anomalous diffusion has also been studied through complex simulation schemes involving obstacles of varying sizes and spatial distribution [37,38]. We will not consider such models for the sake of simplicity.

C. Superdiffusion

At the macroscopic level, the main type of active intracellular transport involves molecular motors which carry particles (cargo) along microtubular filament tracks. The molecular motors and their cargo undergo superdiffusion on a network of microtubules in order to reach a specific area quickly. The molecular motor moves step by step along the microtubules

due to a mechanicochemical energy transduction process. A single step of the molecular motor is modeled by the so-called Brownian ratchet [39]. When we observe the motion of the molecular motor along a filament on longer timescales (several steps), its dynamic can be approximated by a Brownian motion with constant drift (also called directed Brownian motion) [40,41].

The Brownian motion with drift is a solution of the SDE,

$$dX_t^i = v_i dt + \sigma dB_t^{1/2,i}, \quad i = 1,2, \tag{10}$$

where $v = (v_1, v_2) \in \mathbb{R}^2$ is the constant drift parameter modeling the velocity of the molecular motor. The MSD of the directed Brownian motion is given by

$$\mathrm{MSD}(t) = \|v\|^2 t^2 + 2\sigma^2 t \geqslant 2\sigma^2 t. \tag{11}$$

It is superlinear and thus defines a superdiffusion. Superdiffusion can also be modeled by fractional Brownian motion with the Hurst parameter $1/2 < \mathfrak{h} < 1$. Its MSD is given by (9), as we already said. However, this time it is superlinear as $\beta = 2\mathfrak{h} > 1$. Then fractional Brownian motion with $1/2 < \mathfrak{h} < 1$ is an anomalous superdiffusion. However, we note that in the biophysics literature the use of the fractional Brownian motion is mainly related to anomalous subdiffusion.

III. STATISTICAL TEST PROCEDURE FOR A SINGLE TRAJECTORY

We suppose that the trajectory $\mathbb{X}_n = (X_{t_0}, \ldots, X_{t_n})$ is generated from some unknown diffusion process X_t solution of the SDE (3). Our procedure allows us to test from which type of diffusion the observed trajectory is generated.

We derive two hypothesis-testing procedures: one for testing H_0 (X_t is a free diffusion) versus H_1 (X_t is a subdiffusion) and the second for testing H_0 (X_t is a free diffusion) versus H_2 (X_t is a superdiffusion). Then we aggregate the two procedures to build a three-decision procedure.

A. Test statistic

Let us consider the standardized maximal distance T_n of the process from its starting point

$$T_n = \frac{D_n}{\sqrt{(t_n - t_0)\hat{\sigma}_n^2}}, \tag{12}$$

where D_n is the maximal distance of the process from its starting point

$$D_n = \max_{i=1,\ldots,n} \left\| X_{t_i} - X_{t_0} \right\|_2 \tag{13}$$

and $\hat{\sigma}_n$ is a consistent estimator of σ. The choice of $\hat{\sigma}$ is discussed in Sec. III D. If T_n is small, it means the process stays close to its initial position during the period $[t_0, t_n]$; it is likely that it is a subdiffusion. On the contrary, if T_n is large, it means the process goes away from its starting point as a superdiffusion does with high probability. It is worth noting that T_n can be related to the mean maximum excursion second moment proposed by Tejedor *et al.* [42] as an alternative to the MSD. Now this measure introduces an order in the diffusion process solution of the SDE (3). Then it allows us to classify them into the different classes of diffusion, i.e., free diffusion, superdiffusion, and subdiffusion. We want to build a test whose null hypothesis is that the trajectory comes from a Brownian motion (equivalently a free diffusion), a very popular process in biophysics. As a consequence, T_n must be a pivotal statistic under the hypothesis H_0 that is the trajectory is Brownian.

Lemma 1. Let $\hat{\sigma}_n$ be a consistent estimator of σ such that the distribution of $\hat{\sigma}_n/\sigma$ does not depend on σ. If X_t is a Brownian motion, the distribution of T_n does not depend on σ.

Let $q_n(\alpha)$ be the quantile of T_n of order $\alpha \in (0,1)$ when X_t is a Brownian motion. From Lemma 1, $q_n(\alpha)$ does not depend on σ.

B. Two-hypothesis-test procedure derived from the test statistic

First we define $\phi_{1,\alpha}$ as the hypothesis test associated with H_0 versus H_1 at the level $\alpha \in (0,1)$. The procedure $\phi_{1,\alpha}$ is defined through its critical region

$$\mathcal{R}_{1,\alpha} = \{T_n < q_n(\alpha)\} \tag{14}$$

as

$$\phi_{1,\alpha}(\mathbb{X}_n) = \begin{cases} 1 & \text{if } \mathbb{X}_n \in \mathcal{R}_{1,\alpha} \\ 0 & \text{otherwise.} \end{cases}$$

Then T_n has the probability α to lie in the critical region (14). According to Lemma 1, the level of the test $\phi_{1,\alpha}$ is α,

$$\sup_{\sigma>0} P_{1/2,0,\sigma}(T_n < q_n(\alpha)) = \alpha, \tag{15}$$

where $P_{1/2,0,\sigma}$ is the probability measure under the Brownian hypothesis. In fact, as we already mentioned, Brownian motion is the solution of the SDE (3) with $\mathfrak{h} = 1/2$, $\mu = (0,0)$, and diffusion coefficient $\sigma > 0$.

In a similar way, we can perform the test $\phi_{2,\alpha}$ by replacing subdiffusion by superdiffusion in the alternative hypothesis. The associated critical region is

$$\mathcal{R}_{2,\alpha} = \{T_n > q_n(1-\alpha)\}. \tag{16}$$

C. Three-decision-test procedure

From the two tests $\phi_{1,\alpha/2}$ and $\phi_{2,\alpha/2}$, we define a procedure ϕ as follows:

$$\begin{aligned} &\text{we decide } H_1 \text{ if } \mathbb{X}_n \in \mathcal{R}_{1,\alpha/2}; \\ &\text{we decide } H_2 \text{ if } \mathbb{X}_n \in \mathcal{R}_{2,\alpha/2}; \\ &\text{we do not reject } H_0 \text{ otherwise.} \end{aligned} \tag{17}$$

This procedure is well defined since the intersection of the critical regions $\mathcal{R}_{1,\alpha}$ and $\mathcal{R}_{2,\alpha}$ is empty. This procedure is a three-decision-test procedure and admits three kinds of errors (see Table I).

The first kind of error is to reject the null hypothesis H_0 while H_0 is actually true. The probability that this error occurs

TABLE I. The three kinds of error in a three-decision-test procedure.

Truth\Decision	Do not reject H_0	Decide H_1	Decide H_2
H_0 true	no error	type I	type I
H_1 true	type II	no error	type III
H_2 true	type II	type III	no error

is the level of the test, which is defined as

$$\sup_{\sigma>0} \mathbb{E}_{1/2,0,\sigma}(\phi_{1,\alpha} + \phi_{2,\alpha}) = \alpha, \tag{18}$$

where $\mathbb{E}_{1/2,0,\sigma}$ is the expectation operator under the Brownian hypothesis. We only control the occurrence of this first kind of error. Then we note that acceptance of H_0 (X_t is a free diffusion) does not necessarily demonstrate that H_0 is true. It only means that data do not show any evidence against the null hypothesis. Ultimately, we reject this assumption in favor of one of the alternatives at level $\alpha/2$.

The second type of error occurs when we do not reject the null hypothesis while one of the alternatives is true.

The last type of error is to reject the null hypothesis in favor of a wrong alternative. In the literature of three-decision tests such an error is called a type III error (see, for example, [43] and references therein).

D. Choosing the estimator of σ

Ideally, we would like to find an estimator of σ which is consistent according to the large-sample scheme under the hypotheses H_0, H_1, and H_2 and satisfies the assumption that the distribution of $\hat{\sigma}_n/\sigma$ is free of σ under H_0. However, the large-sample scheme is not favorable to get an estimator with such properties. For instance, Florens-Zmirou [44] shows that the naive maximum-likelihood estimator for the drift parameter has an asymptotic bias of the order of the lag time Δ. Thus, the high-frequency scheme and the rapidly increasing design turn out to be more convenient to provide consistent estimators. In fact, in the limit, these schemes correspond to the situation in which we have a continuous observation of the process on the time interval of observation. Jiang and Knight [45] propose nonparametric estimators of both the drift and the diffusion coefficient. The consistency of these estimators is proven under the high-frequency scheme only. Therefore, in this section we discuss the estimation of the diffusion coefficient under the large sample scheme.

The first proposition to estimate σ may be

$$\hat{\sigma}_{1,n}^2 = \frac{1}{2n\Delta} \sum_{j=1}^{n} \left\| X_{t_j} - X_{t_{j-1}} \right\|_2^2. \tag{19}$$

Even if the estimator (19) is strongly consistent under the high-frequency scheme for every process X_t solution of (3) [46], the following proposition tells us that it is not the case under the large-sample scheme.

Proposition 1.

(a) Under H_0, $\hat{\sigma}_{1,n}$ is strongly consistent and the distribution of $\hat{\sigma}_{1,n}/\sigma$ is free of σ.

(b) If X_t is an Ornstein-Uhlenbeck process (6), $\hat{\sigma}_{1,n}^2/\sigma^2$ converges in probability to $(1 - e^{-\lambda\Delta})/\lambda\Delta$.

(c) If X_t is a Brownian motion with drift (10), $\hat{\sigma}_{1,n}^2/\sigma^2$ converges almost surely to $\Delta\|v\|_2^2/2\sigma^2 + 1$.

(d) If X_t is a fractional Brownian motion (8), $\hat{\sigma}_{1,n}^2/\sigma^2$ converges almost surely to $\Delta^{2\mathfrak{h}-1}$.

A proof of Proposition 1 is given in Appendix A 2. Proposition 1 states that $\hat{\sigma}_{1,n}$ is adequate for our procedure under the null hypothesis in the large sample scheme. However, $\hat{\sigma}_{1,n}$ is asymptotically biased under some alternatives (again in the large sample scheme). Notice that if X_t is an Ornstein-Uhlenbeck process (6), then $\hat{\sigma}_{1,n}^2$ underestimates σ^2 on average since $(1 - e^{-x})/x < 1$ for $x > 0$. Then T_n might be overvalued with this estimator, increasing the type II or type III error rate in our procedure. If X_t is a Brownian motion with drift (10), $\hat{\sigma}_1^2$ overestimates σ^2 on average. Then T_n might be undervalued with this estimator, increasing the type II or type III error rate. For fractional Brownian motion (8), the ratio $\hat{\sigma}_{1,n}^2/\sigma^2$ is inhomogeneous and depends on the value of Δ. Let us assume $\Delta < 1$. For subdiffusive fractional Brownian motion ($\mathfrak{h} < 1/2$), we can show that $\hat{\sigma}_{1,n}^2$ overestimates σ^2 in average as $\Delta^{2\mathfrak{h}-1} > 1$ for $\mathfrak{h} < 1/2$. Then T_n might be undervalued with this estimator, decreasing type II or type III error rate in our procedure. For superdiffusive fractional Brownian motion ($\mathfrak{h} > 1/2$), we can show that $\hat{\sigma}_{1,n}^2$ underestimates σ^2 in average as $\Delta^{2\mathfrak{h}-1} < 1$ for $\mathfrak{h} > 1/2$. Then T_n might be overvalued with this estimator, decreasing type II or type III error rate in our procedure. Then the bias of $\hat{\sigma}_{1,n}^2$ can be favorable to our procedure for certain alternatives (fractional Brownian motion with $\Delta < 1$) and defavorable for others (Ornstein-Uhlenbeck and Brownian motion with drift).

The second suggestion to estimate σ may be based on the second-order differences rather than the first-order differences,

$$\hat{\sigma}_{2,n}^2 = \frac{1}{2n\Delta} \sum_{j=1}^{n-1} \left\| \left(X_{t_{j+1}} - X_{t_j}\right) - \left(X_{t_j} - X_{t_{j-1}}\right) \right\|_2^2. \tag{20}$$

Like $\hat{\sigma}_{1,n}^2$, $\hat{\sigma}_{2,n}^2$ fulfills the assumption of Lemma 1 under H_0. This estimator has the advantage of decreasing the bias under some alternatives. For instance, it removes the bias in the case of Brownian motion with drift.

E. Approximation of the distribution of the statistic under the null hypothesis and asymptotic behavior of our procedure

In this paragraph, we emphasize again that we study the asymptotic under the large sample scheme: The interobservation time Δ remains fixed and the number of observations n tends to infinity. The following theorem gives the asymptotic behavior of our procedure under the null hypothesis.

Theorem 1. Let X_t be a Brownian motion on $\mathbb{R}^2$. Let $\hat{\sigma}_n$ be a consistent estimator of the diffusion parameter σ of X_t. The test statistic T_n converges in distribution to $S_0 = \sup_{0\leqslant s\leqslant 1} \|W_s\|_2$ as $n \to \infty$. Here W_t is a standard two-dimensional Brownian motion that is the Brownian motion of variance $\mathbf{I}_2$ and initialization $W_0 = (0,0)^\top$.

A proof of Theorem 1 is given in Appendix A 1. The limit distribution of the test statistic under H_0 admits an analytical form [47]

$$x \in (0, +\infty) \to \sum_{k=1}^{\infty} \frac{2e^{-j_{0,k}^2/2x^2}}{j_{0,k} J_1(j_{0,k})},$$

where $x \geqslant 0$, J_ν is the Bessel function of order ν, and $0 < j_{\nu,1} < j_{\nu,2} < \cdots$ are the positive zeros of J_ν. Replacing the quantiles $q_n(\alpha)$ by the quantiles of S_0 in our test procedure provides us with a test of the asymptotic level α.

Furthermore, the following proposition gives the asymptotic behavior of the test statistic under parametric alternatives

TABLE II. Estimation of the quantiles of order $\alpha/2$ and $1-\alpha/2$ ($\alpha = 5\%$) for different trajectory lengths n, using Algorithm 1 (Appendix B) with $N = 1\,000\,001$.

	Trajectory size			
Quantile order	10	30	100	Asymptotic
2.5%	0.725	0.754	0.785	0.834
97.5%	2.626	2.794	2.873	2.940

when the estimator $\hat{\sigma}_{1,n}$ is considered (see Appendix A 3 for a proof). More generally, as long as the estimator $\hat{\sigma}_n$ of the diffusion coefficient is such that $\hat{\sigma}_n/\sigma$ converges in probability to a positive constant whatever the dynamic of X_t, then the following proposition holds.

Proposition 2. Assume that we consider the estimator (19) in our procedure (12).

(a) If X_t is an Ornstein-Uhlenbeck process (6), T_n converges in probability to 0.

(b) If X_t is a fractional Brownian motion (8) with $0 < \mathfrak{h} < 1/2$, T_n converges in probability to 0.

(c) If X_t is a fractional Brownian motion (8) with $1/2 < \mathfrak{h} < 1$, T_n converges in probability to $+\infty$.

(d) If X_t is a Brownian motion with drift (10), T_n converges in probability to $+\infty$.

Note that Theorem 1 and Proposition 2 allow us to control the error rates of type II and type III under parametric alternatives; the associated error rates converge to 0 with n.

However, as in practice n may be small, the asymptotic approximation of the quantiles of T_n may not be accurate. Then the level of the test is no longer α. Since we are able to draw a sample from the distribution of T_n under H_0 (see Algorithm 1), we propose a Monte Carlo estimate of the quantile $q_n(x)$, $0 < x < 1$. This estimate is defined as the $[xN]$th-order statistic $q_n^{(N)}(x)$ of the sample $(T_n^{(1)}, \ldots, T_n^{(N)})$. Table II shows that there is a significant difference between asymptotic and nonasymptotic quantiles. As expected, as $n \to \infty$, $q_n(\alpha)$ converges to the quantile of S_0 of order α (column Asymptotic in Table II).

Algorithm 1. Simulation of an N sample $(T_n^{(1)}, \ldots, T_n^{(N)})$ of the distribution of the statistic T_n under H_0.

Input: n, α, and L
// the length n of the trajectory
// the probability $\alpha \in (0,1)$
// the number N of Monte Carlo experiments
Result: $q_n^{(N)}(\alpha)$
for $i = 1$ **to** N **do**
// Simulation of a Brownian trajectory of size n, of variance $\sigma = 1$, and with resolution time $\Delta = 1$.
initialization $Y_0^{(i)} = (0,0)^\top$;
for $j = 1$ **to** n **do**
Draw $\epsilon \sim \mathcal{N}(0, \mathbf{I_2})$;
$Y_j^{(i)} = Y_{j-1}^{(i)} + \epsilon$;
end
// Computation of the test statistic
Compute the ratio $T_n^{(i)} = D_n^{(i)}/\hat{\sigma}_n^{(i)}$ from $(Y_0^{(i)}, \ldots, Y_n^{(i)})$;
end

In dealing with a test, we can also be interested in computing the p value. The p value of the test H_0 vs H_1 (subdiffusion as the alternative) is defined as

$$p_{1,n} = F_n(T_n), \tag{21}$$

where F_n denotes the cumulative distribution function of T_n under H_0. The p value of the test H_0 vs H_2 (superdiffusion as the alternative) is defined as

$$p_{2,n} = 1 - F_n(T_n). \tag{22}$$

Testing the hypothesis H_0 vs the hypothesis H_1 or H_2 is more tricky as we use a two-sided test with a nonsymmetric distribution. In this case we can define the p value as

$$p_n = 2\min\{p_{1,n}, p_{2,n}\}. \tag{23}$$

Doubling the lowest one-tailed p value can be seen as a correction for carrying out two one-tailed tests. We estimate F_n with the standard empirical distribution function estimated by Monte Carlo simulations using Algorithm 1,

$$\hat{F}_n(x) = N^{-1}\sum_{i=1}^{N} \mathbf{1}\big(T_n^{(i)} \leqslant x\big), \tag{24}$$

where $\mathbf{1}(A)$ is the indicator function of event A. Then we estimate the p value (23) replacing F_n with $\hat{F}_n$.

IV. MULTIPLE-TEST PROCEDURE FOR A POPULATION OF TRAJECTORIES

Trackers compute a collection of particle trajectories from a sequence of images. Thus, it is desirable to decide the modes of mobility for a collection of particle trajectories. For now, we consider a collection $\mathcal{X}_m$ of m trajectories which are simultaneously observed. We denote by $\mathbb{X}_{n_k}^{(k)}$ the observations associated with the kth particle,

$$\mathbb{X}_{n_k}^{(k)} = \big(X_{t_0}^{(k)}, \ldots, X_{t_{n_k}}^{(k)}\big), \quad k = 1, \ldots, m,$$
$$\mathcal{X}_m = \big\{\mathbb{X}_{n_k}^{(k)}, k = 1, \ldots, m\big\}.$$

We assume that the observed trajectories are independent. For all trajectories $k = 1, \ldots, m$, we derive our trichotomy-hypothesis-test procedure: $H_0^{(k)}$ ($X_t^{(k)}$ is a free diffusion) versus $H_1^{(k)}$ ($X_t^{(k)}$ is a subdiffusion) or $H_2^{(k)}$ ($X_t^{(k)}$ is a superdiffusion). We are faced with the problem of simultaneous tests when the rejections of null hypotheses $H_0^{(k)}$ are accompanied by claims of the direction of the alternative ($H_1^{(k)}$ or $H_2^{(k)}$). In this setup, multiple-test procedures are preferable over single-test procedures. Indeed, applying the procedure at level α for each trajectory produces on average a number of $m\alpha$ type I errors. A multiple-testing procedure aims to control the number of false discoveries. We refer the reader to [48–50] for a review.

A multiple-testing procedure of m null hypotheses against two alternative hypotheses is a rule $\mathcal{R}_1(\mathcal{X}_m) \times \mathcal{R}_2(\mathcal{X}_m)$, where $\mathcal{R}_1(\mathcal{X}_m)$ and $\mathcal{R}_2(\mathcal{X}_m)$ are disjoint subsets of $\{H_0^{(1)}, \ldots H_0^{(m)}\}$. For $i = 1,2$, $\mathcal{R}_i(\mathcal{X}_m)$ is the set of the rejected hypotheses $H_0^{(k)}$ to the benefit of the alternative $H_i^{(k)}$. We may commit three kinds of errors in such a multiple-testing procedure. Let us introduce the following notation before listing these errors. We denote by m_0 the number of true hypotheses $H_0^{(k)}$. In our context m_0 is the

TABLE III. Outcomes in testing m null hypotheses against two alternatives. For $i = 1,2$, R_i is the cardinal of $\mathcal{R}_i(\mathcal{X}_m)$. The variables $(S_i)_{i=1,\ldots,4}$, $(T_i)_{i=1,2}$, U, and $(V_i)_{i=1,2}$ are not observed and depend on $\mathcal{X}_m$ and P.

Truth\Decision	Accept H_0	Accept H_1	Accept H_2	Total
H_0	U	V_1	V_2	m_0
H_1	T_1	S_1	S_3	m_1
H_2	T_2	S_4	S_2	m_2
Total	$m - R_1 - R_2$	R_1	R_2	m

number of true Brownian trajectories. We emphasize that m_0 is an unobservable random variable. We define by $R = R_1 + R_2$ the observed number of null hypotheses which are rejected by the multiple-testing procedure. Table III summarizes the number of errors which may occur following a multiple-testing procedure.

(a) We make a type I error on $H_0^{(k)}$ when we reject $H_0^{(k)}$ while it is a true null hypothesis. The number of errors of the first kind is $V = V_1 + V_2$.

(b) A type II error occurs when we do not reject a null hypothesis $H_0^{(k)}$ while $H_0^{(k)}$ is false. The number of errors of the second kind is $T = T_1 + T_2$.

(c) The type III errors are directional errors: The hypothesis $H_0^{(k)}$ is correctly rejected $[k \in \mathcal{R}_1(\mathcal{X}_m) \cup \mathcal{R}_2(\mathcal{X}_m)]$, but for the wrong alternative. We mix up the alternatives deciding one while it is the other. The number of errors of the third kind is $S = S_3 + S_4$.

To measure the type I error rate, it is common to consider the k familywise error rate (FWER) or the FDR (see [49] and references therein). In our settings, controlling the type I error rate is a first step, but it would be necessary to control type III errors as well. In the literature, the sum of the number of errors of the first and third kinds is controlled using the mixed-directional familywise error rate (MDFWER) or the mixed-directional false discovery rate (MDFDR) (see [48]). The MDFWER and MDFDR are only controlled for the problem of testing null hypotheses against two-sided alternatives for finite-dimensional parameters (see, for example, [51] and references therein).

Biologists are interested in the proportions of each dynamic (subdiffusion, superdiffusion, and Brownian motion) and their geographic location in the cell. In this context, controlling the FWER, that is, the probability of making a single false discovery, is not relevant. That is why we focus on a procedure which enables us to control the FDR. Guo and Romano (see [51], Sec. 5) also present several multiple-test procedures associated with three-decision problems which aim to control the FDR. Their approach is different since the problem is rewritten as a problem which carries out $3m$ null hypotheses. Their proposed procedures control strongly the FDR only on $2m$ null hypotheses among the $3m$ under the dependence or independence of the test statistics. In this section we propose to adapt the multiple-testing procedures of Benjamini and Hochberg [52] and Benjamini and Hochberg [28] controlling the FDR that is the average proportion of false discoveries among the discoveries. We stress that our model is nonparametric. Then we will consider the control of the MDFDR or MDFWER for a next issue.

Let $p^{(k)}$, $p_1^{(k)}$, and $p_2^{(k)}$ be, respectively, the p value (23), (21), and (22) associated with the kth trajectory, $k = 1, \ldots, m$. Let $p^{(1:m)} \leqslant p^{(2:m)} \leqslant \cdots \leqslant p^{(m:m)}$ be the ordered p values $p^{(k)}$, and $H_0^{(1:m)}, \ldots, H_0^{(m:m)}$ the associated null hypotheses. The adaptation of the Benjamini-Hochberg (BH) procedure is described in the following procedure.

Procedure 1.

(a) Use the Benjamini-Hochberg procedure on the p values $(p^{(k)})_{k=1,\ldots,m}$: (i) Let $k^\star$ be the largest k for which $p^{(k:m)} \leqslant \frac{k}{m}\alpha$ and (ii) let $\mathcal{R}_\alpha(\mathcal{X}_m)$ be the set of hypotheses $\{H^{(1:m)}, H^{(2:m)}, \ldots, H^{(k^\star:m)}\}$.

(b) Let $\mathcal{R}_{1,\alpha}(\mathcal{X}_m)$ be the subset $\mathcal{R}_\alpha(\mathcal{X}_m)$ such that $p_1^{(k)} < p_2^{(k)}$.

(c) Let $\mathcal{R}_{2,\alpha}(\mathcal{X}_m)$ be the subset $\mathcal{R}_\alpha(\mathcal{X}_m)$ such that $p_1^{(k)} > p_2^{(k)}$.

The set $\mathcal{R}_\alpha(\mathcal{X}_m)$ is the set of all rejected null hypotheses for our trichotomy test. According to Finner and Roters [53], we have

$$\mathrm{FDR}[\mathcal{R}_\alpha(\mathcal{X}_m)] = \mathbb{E}\left(\frac{V}{\max(R,1)}\right) = \frac{m_0}{m}\alpha,$$

where $\mathbb{E}$ is the expectation associated with the m-tuplet stochastic processes $(X_t^{(k)}, k = 1, \ldots, m)$ which generates the m trajectories. Then the FDR of Procedure 1 is controlled by α. Moreover, the p values $p_1^{(k)}$ and $p_2^{(k)}$ give the information to which side of the distribution F_{n_k} the associated test statistic $T_{n_k}^{(k)}$ is. The case of equality ($p_1^{(k)} = p_2^{(k)} = 1/2$) never occurs since such a null hypothesis will not be rejected at step (a) of Procedure 1.

Actually, we may also use the adaptive BH procedure of [28] as the first step of Procedure 1. Thus Procedure 1 will be referred to as the adaptive (standard) Procedure 1 when we use the adaptive (standard) BH procedure as the first step. The adaptive BH procedure is more powerful than the standard BH procedure. It uses an estimation of the number of true null hypotheses m_0 to increase the power of the BH procedure. Benjamini and Hochberg [28] simply define the adaptive BH procedure by replacing m by an estimator $\hat{m}_0$ of m_0 in the BH procedure. The associated FDR is $(m_0/\hat{m}_0)\alpha$ and is less than α if $\hat{m}_0 \leqslant m_0$ almost surely.

The procedure to estimate m_0 presented in [28] is made for $\hat{m}_0$ to be upward biased. This bias favors the control of the FDR at level α. Due to the fact that $\hat{m}_0$ does not fulfill the condition $\hat{m}_0 \leqslant m_0$ almost surely, we cannot say that the adaptive BH procedure controls the FDR at level α theoretically. However, simulations from [28] suggest that the adaptive BH procedure controls the FDR at level α. Based on simulations (see Table V), we show that Procedure 1 also controls the MDFDR defined as $\mathbb{E}[(V + S)/\max(R,1)]$.

V. SIMULATION STUDY AND APPLICATION TO REAL MICROSCOPY DATA

We assess the power of our single-test procedure (on a single trajectory) and our multiple-test procedure (on a collection of trajectories) by Monte Carlo simulations. We consider

parametric alternatives: the Ornstein-Uhlenbeck (6) and the fractional Brownian motion with Hurst index $0 < \mathfrak{h} < 1/2$ for subdiffusion processes (H_1) and the Brownian motion with drift (10) and the fractional Brownian motion with Hurst index $1/2 < \mathfrak{h} < 1$ for superdiffusion processes (H_2). Then we apply our procedure to real data, comparing our results with those obtained due to a method based on the mean-square displacement.

A. Power of the test procedure for a single trajectory

The power is defined as the probability of accepting the alternative hypothesis H_i, $i = 1,2$, when H_i is effectively true. Thus, the higher the power (ideally the closest to 1), the better the test procedure can discriminate correctly the hypotheses. In what follows, Fig. 3 (and Fig. 13 in Appendix B) display the power under parametric alternatives for a range of values of the parameter and for different trajectory sizes. For instance, when the alternative hypothesis H_1 is the Ornstein-Uhlenbeck process (6), the power is defined as the function f:

$$f(\lambda,n) = P(\mathbb{X}_n(\lambda) \in \mathcal{R}_{1,\alpha/2} | H_1 \text{ is true}), \qquad (25)$$

where $\mathbb{X}_n(\lambda)$ denotes a trajectory of size n from an Ornstein-Uhlenbeck process (6) of the parameter λ. We recall that the event $\{\mathbb{X}_n(\lambda) \in \mathcal{R}_{1,\alpha/2}\}$ means that the three-decision test accepts hypothesis H_1 at level α for the trajectory $\mathbb{X}_n$ [see Eq. (17)]. As expected, the power of the test under parametric alternatives converges to 1 with n (see Fig. 3 as well as Fig. 13 in Appendix B). This property is a consequence of Proposition 2 for the mentioned alternatives. Indeed, the larger the trajectory size n is, the more information we have about the trajectory and the better the test detects the alternative hypothesis H_i, $i = 1,2$, when H_i is true. Thus, a power curve corresponding to a test on long trajectories (large n) will be above the power curve corresponding to a test on short trajectories (small n). On the other hand, in statistical testing, it is well known that the further from the null hypothesis the process is (for instance, λ chosen far from 0 for an Ornstein-Uhlenbeck process), the higher the power is.

If X_t is an Ornstein-Uhlenbeck process (6) which is entered in its stationary regime, then the distribution of the test statistic does not depend on θ (see Appendix A 4). Figure 3(b) shows the plot of the power regarding the values of λ which models the strength of the restoring force toward the equilibrium position θ. The power function is an increasing function of λ. The larger λ is, the stronger is the restoring force and then the better the test will detect correctly the alternative hypothesis H_1. In short, the stronger the force is, more powerful the test is.

Furthermore, if X_t is a Brownian motion with drift with parameters v and σ such that $\|v\|\sqrt{\Delta} > \sigma$, then the particle goes toward the direction of v while the Brownian random part of the SDE (10) does not affect much its trajectory (see Appendix A 4). Consequently, the trajectory looks quite straight and the test has a high probability of detecting it as a superdiffusion (hypothesis H_2). In other words, the larger the norm of the drift parameter v is compared to σ, more powerful the test is [see Fig. 3(a)].

If X_t is a fractional Brownian motion, then the distribution of T_n depends only on the Hurst index $\mathfrak{h}$ (see Appendix A 4). Then the test procedure is equivalent to test the null hypothesis

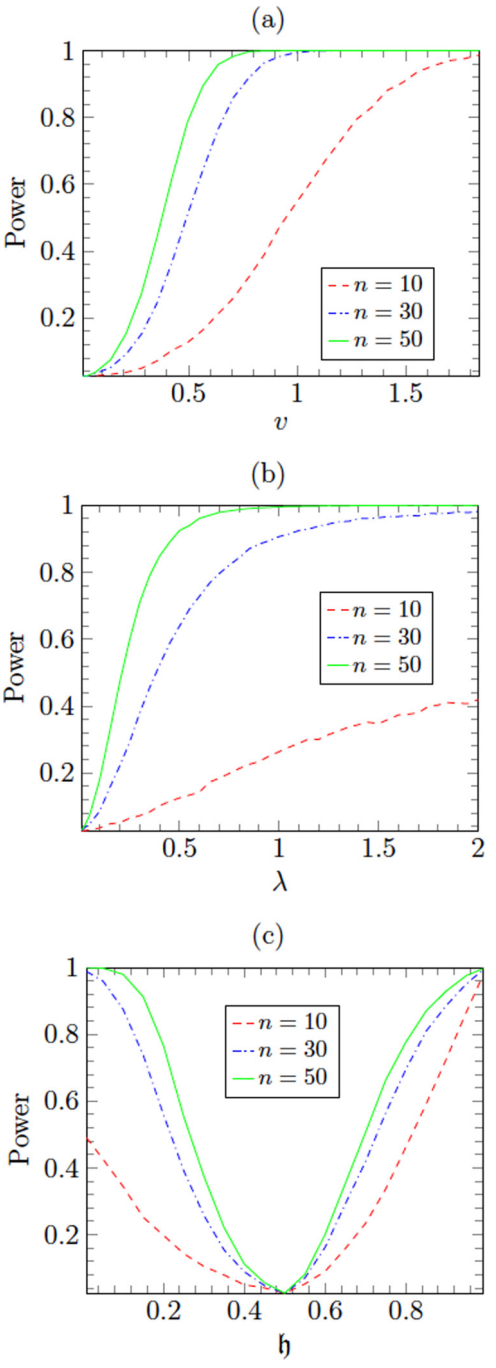

FIG. 3. Monte Carlo estimate of the power of the test at level $\alpha = 0.05$ according to the trajectory length n and the parameter associated with the following parametric alternatives: (a) Brownian motion with drift [with the parameter $v = (v_1, v_2)$ such that $v_1 = v_2$], (b) the Ornstein-Uhlenbeck process (parameter λ), and (c) fractional Brownian motion (parameter $\mathfrak{h}$). We use 10 001 Monte Carlo replications to compute each point of the power curves.

$\mathfrak{h} = 1/2$ (corresponding to the Brownian hypothesis) versus $\mathfrak{h} \neq 1/2$ [see Fig. 3(c)]. When $0 < \mathfrak{h} < 1/2$ (subdiffusive process), low values of $\mathfrak{h}$ correspond to a process whose MSD has a low exponent β [$\text{MSD}(t) \propto t^{\beta}$; see Eq. (9)]. Therefore, the lower $\mathfrak{h}$ is, the more subdiffusive the trajectory is and the better the test detects correctly subdiffusion: The power

TABLE IV. Parameters used for simulating the alternative hypotheses. For simplicity, we took $\sigma = 1$ for all processes (including Brownian motion). We chose $\Delta = 1$.

Hypothesis	Process	Parameter	Value
H_1	Ornstein-Uhlenbeck	λ	0.53
H_1	fractional Brownian	$\mathfrak{h}$	0.13
H_2	Brownian motion with drift	$\|v\|$	0.66
H_2	fractional Brownian	$\mathfrak{h}$	0.85

function is decreasing for $\mathfrak{h} \in (0,1/2)$. On the contrary, when $\mathfrak{h} > 1/2$ (superdiffusive process), large values of $\mathfrak{h}$ correspond to a process whose MSD has a large exponent β. The larger $\mathfrak{h}$ is, the more superdiffusive the trajectory is and the better the test detects correctly superdiffusion: The power function is increasing for $\mathfrak{h} \in (1/2,1)$.

Appendix B explores the case where the process is a subdiffusion modeled by a continuous-time random walk. The corresponding power curves are plotted in Fig. 13 (Appendix B).

As a concluding remark, we observe that under all the parametric alternatives studied here, the power corresponding to a trajectory size $n = 10$ is significantly lower compared to $n = 30,50$. Thus, we argue that it is very hard to classify accurately a trajectory with fewer than ten points, as we have very little information about the dynamics in this case.

B. Average power and the MDFDR of the multiple-test procedure for a collection of trajectories

The simulation settings are described as follows. According to experience, we choose the number of trajectories to be $m = 100$ or 200. All the trajectories are assumed to have the same size $n = 30$, since this size is reasonable regarding real data. The diffusion coefficient σ and the lag time Δ are set to 1. The collection of trajectories $\mathcal{X}_m$ is composed of $m_0 < m$ Brownian trajectories (H_0); $(m - m_0)/2$ subdiffusive trajectories (H_1), half from an Ornstein-Uhlenbeck process with parameter $\lambda > 0$ and half from a fractional Brownian motion with Hurst index $0 < \mathfrak{h} < 1/2$; and $(m - m_0)/2$ superdiffusive trajectories (H_2), half from a Brownian motion with drift $v \in \mathbb{R}^2$ and half from a fractional Brownian motion with Hurst index $1/2 < \mathfrak{h} < 1$. The parameters to simulate these trajectories are given in Table IV. We take the parameters corresponding to a power of the single-test procedure of 80%. Such parameters are used to produce Fig. 1(a). This choice seems coherent in regard to trajectories from real data [see Fig. 1(b)]. To better picture the trajectories, we show the spread of the exponent β, a commonly used descriptor of the data in biophysics, in Fig. 4 (for the fractional Brownian motion only). For a given m, the proportion of true null hypotheses H_0 varies: $m_0/m \in \{0,0.2,0.4,0.6,0.8\}$.

The MDFDR is a rate which controls the error of type I and type III. It is defined as $\mathbb{E}[(V + S)/\max(R,1)]$ (see Table III). Table V shows that Procedure 1 also controls the MDFDR. The MDFDR and FDR appear to be very close, meaning that the number of type III errors is extremely low. Furthermore, the adaptive Procedure 1 (where m_0 is estimated) is less conservative than the standard Procedure 1. As expected,

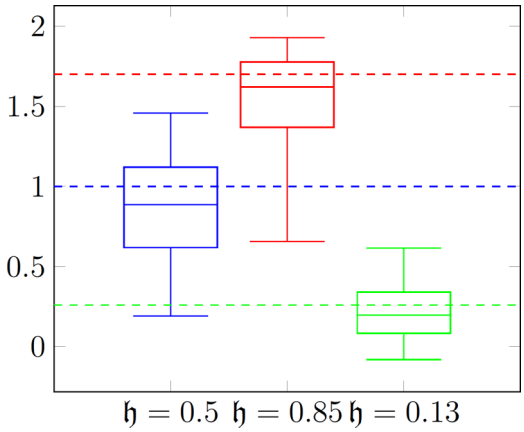

FIG. 4. Box plots of the estimated exponent $\hat{\beta}$. From left to right, we plot the box plot of $\hat{\beta}$ corresponding to Brownian trajectories ($\mathfrak{h} = 1/2$), subdiffusive fractional Brownian trajectories ($\mathfrak{h} = 0.13$), and superdiffusive fractional Brownian trajectories ($\mathfrak{h} = 0.85$). The trajectory size is $n = 30$. Here $\hat{\beta}$ is obtained by linear regression from the log(MSD) curve. We use the first 25 points of the MSD curve to estimate β. The dashed lines correspond to the true β for each situation. We recall that in the case of fractional Brownian motion of the parameter $\mathfrak{h}$ we have $\beta = 2\mathfrak{h}$.

the FDR and MDFDR increase as the proportion of true null hypotheses increases.

To assess the performance of our multiple-test procedure, we use the average power [48]

$$\mathbb{E}\left(\frac{S_i}{m_i}\right), \quad i = 1,2, \tag{26}$$

where m_i is the number of true alternatives H_i and S_i ($i = 1,2$) is defined in Table III. In our simulation scheme, we set $m_i = (m - m_0)/2$. The average power is the expected proportion of hypotheses accepted as H_i among all true alternatives H_i. Then a perfect multiple-test procedure would have an average power equal to one. Average powers of the different simulations corresponding to different values of m_0/m and m are shown in Fig. 5.

TABLE V. Monte Carlo estimate of the FDR and MDFDR for both the standard and adaptive Procedure 1 at level $\alpha = 0.05$. The number of replications is 10 001. The error rate estimations are expressed in percentages.

		Standard		Adaptive	
m	m_0/m	FDR	MDFDR	FDR	MDFDR
100	0	0	0	0	0.2
100	0.2	1	1	3.7	3.7
100	0.4	2.1	2.1	4.2	4.2
100	0.6	3.2	3.2	4.7	4.7
100	0.8	4.1	4.1	4.8	4.8
200	0	0	0	0	0.4
200	0.2	1	1	3.4	3.4
200	0.4	2.1	2.1	4	4
200	0.6	3.2	3.2	4.6	4.6
200	0.8	4	4	4.7	4.7

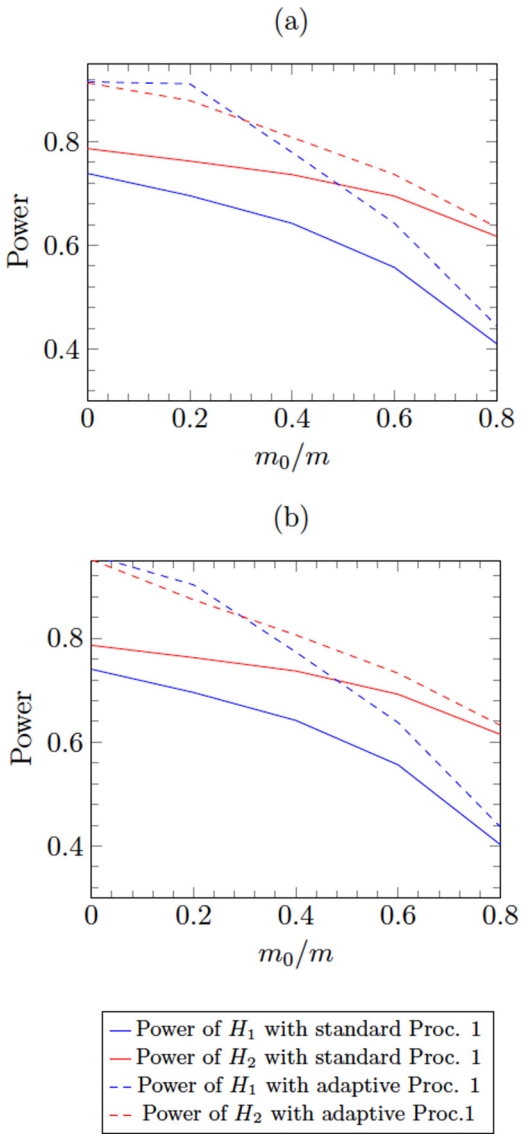

FIG. 5. Monte Carlo estimate of the average power against the proportion of true null hypotheses m_0/m in the collection of hypotheses tested: (a) $m = 100$ hypotheses and (b) $m = 200$ hypotheses.

First, we can see that the powers of H_1 and H_2 are not very sensitive to the number of hypotheses m for both the standard Procedure 1 and the adaptive Procedure 1 [red and blue solid and dashed lines, respectively, which are similar in Figs. 5(a) and 5(b)]. Second, the adaptive Procedure 1 is more powerful than the standard Procedure 1 (red and blue dashed lines, respectively, above the red and blue solid lines in Fig. 5). The benefit of the adaptive Procedure 1 over the standard Procedure 1 decreases as the proportion of true null hypotheses m_0/m increases (solid and dashed lines of the same color getting closer as m_0/m increases in Fig. 5). This is due to the fact that, as m_0/m tends to 1, m_0 and then $\hat{m}_0$ tend to m. As a result, the adaptive and standard versions of Procedure 1 become similar.

Remark 3. We observe that, given a certain procedure (standard or adaptive Procedure 1), the average power of H_1 is lower than the average power of H_2 (see Fig. 5). It is not due to the choice of parameters as both alternatives H_1 and H_2 are simulated to share the same power (80%) as the single-test procedure. Actually, it comes from the fact that the p values under H_2 are stochastically smaller than the p values under H_1 (see Fig. 6). Then the true superdiffusive trajectories are more easily detected as non-Brownian in the first step of the (adaptive) Procedure 1 than the true subdiffusive trajectories. We note that if we use other parametric models for subdiffusion (H_1) and superdiffusion (H_2), we can have the opposite situation.

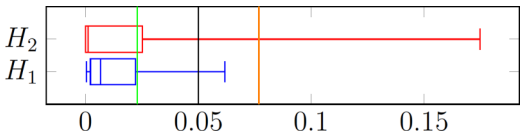

FIG. 6. Box plots of the p value p_{30} [Eq. (23)] under H_1 and H_2. We simulate a set of trajectories $\mathcal{X}_m$ with $m = 100$ and $m_0 = 20$ according to the simulation scheme described in Sec. V. We plot the box plot of the p values $p_{30}^{(i:m)}$ corresponding to each true alternative hypothesis H_1 and H_2. The green (orange) line is the threshold $h = p^{(k^*)}$ obtained by the first step of Procedure 1 (first step of adaptive Procedure 1). The null hypothesis is rejected if the p value is lower than h. The black line is the level $\alpha = 5\%$.

Finally, we compare the adaptive Procedure 1 to the MSD classification of Feder *et al.* [19], based on a fit of the MSD curve to $t \to t^\beta$. We assess the two methods on a single collection of trajectories $\mathcal{X}_m$ with $m = 200$ and $m_0/m = 0.4$, composed of a mixture of Brownian motion, subdiffusion, and superdiffusion as described at the beginning of this section. We get the confusion matrices of Tables VI and VII for, respectively, the MSD method and the adaptive Procedure 1. As suggested by the limiting curves used by Feder *et al.* [19] (see Fig. 2), the MSD method mixes up the Brownian trajectories with both subdiffusion and superdiffusion (see row 1 of Table VI). Another big issue is that 40% of the particles undergoing subdiffusion are considered as immobile by the MSD method. On the other hand, the adaptive Procedure 1 detects well subdiffusion and superdiffusion in the setting of this simulation (rows 2 and 3 of Table VII). More importantly, it controls the number of false discoveries through the FDR (row 1 of Table VII).

C. Real data: The Rab11a protein sequence

Fluorescence imaging and microscopy has a prominent role in life science and medical research. It consists of detecting specific cellular and intracellular objects of interest at the diffraction limit (200 nm). These objects are first tagged with genetically engineered proteins that emit fluorescence, e.g.,

TABLE VI. Confusion matrix for the MSD method.

Truth/Label	Brownian	Subdiffusion	Superdiffusion	Still
Brownian	19	45	36	0
subdiffusion	0	60	0	40
superdiffusion	3	0	97	0
not moving	0	0	0	0

TABLE VII. Confusion matrix for the adaptive Procedure 1.

Truth/Label	Brownian	Subdiffusion	Superdiffusion
Brownian	96	0	4
subdiffusion	23	77	0
superdiffusion	10	0	90

green fluorescent protein (GFP). Then they can be observed using wide-field or confocal microscopy. Several image analysis methods have been developed to quantify intracellular trafficking, including object detection and tracking of fluorescent tags in cells [2,54].

Here we are particularly interested in studying the exocytosis process, which is the mechanism of active transport of proteins out of the cell. Small structures, called vesicles, travel from organelles to the cell membrane, propelled by motor activity. The vesicle fuses with the plasma membrane and delivers the transported protein in the extracellular medium. Given computed trajectories, we investigate here the quantification of vesicle dynamics and trafficking. As explained earlier in the paper, the trajectories can be generally classified into three categories: Brownian motion, subdiffusion, and superdiffusion.

As a model of exocytosis or recycling, we focus on the Rab11a protein. This protein is a member of the dynamic architecture of the complex molecular assembly which regulates recycling organelle trafficking. It plays an essential role in the regulation of late steps of vesicle recycling to the plasma membrane, namely, the tethering-docking process [29]. During exocytosis, Rab11a is attached to the vesicle membrane. Then tracking Rab11a amounts to tracking the vesicle during the exocytosis phase. After the fusion of the vesicle to the cell membrane, Rab11a is recycled in the cytosol. During the recycling step, the tracking of Rab11a is not accurate as the proteins are detached from the vesicle and scatter around the cytosol. It is currently under investigation. For that reason, we focus on the exocytosis process until the fusion time with the cell membrane.

An illustration of the Rab11a sequence is shown in Fig. 7 where the dark spots correspond to Rab11a-GFP vesicles in a "crossbow" micropatterned shape cell. A typical image extracted from an image sequence is shown in Fig. 7. The image sequence is composed of 600 images of size 256×240 (1 pixel = 160 nm) acquired at 10 frames/s ($\Delta = 0.1$ s). All imaging acquisition was carried out in a full conditioned medium at 37 °C and 5% CO_2. Simultaneous dual-color TIRF microscopy sequences were acquired on a Nikon TE2000 inverted microscope equipped with a $100\times$ TIRF objective (numerical aperture equal to 1.49). We tracked 1561 trajectories with the multiple-hypothesis tracking method with default parameters [55], available on the Icy software [56]. However, we discarded too small and too long trajectories corresponding to tracking errors in most cases. Then we have to get rid of the particles that do not move enough and consequently cannot be modeled by diffusion processes. In practice, we analyze only the trajectories with at least 20 distinct positions and the vesicles that stop at the same position less than $K = \lfloor n/10 \rfloor$ times (with n the length of the trajectory). In the case of

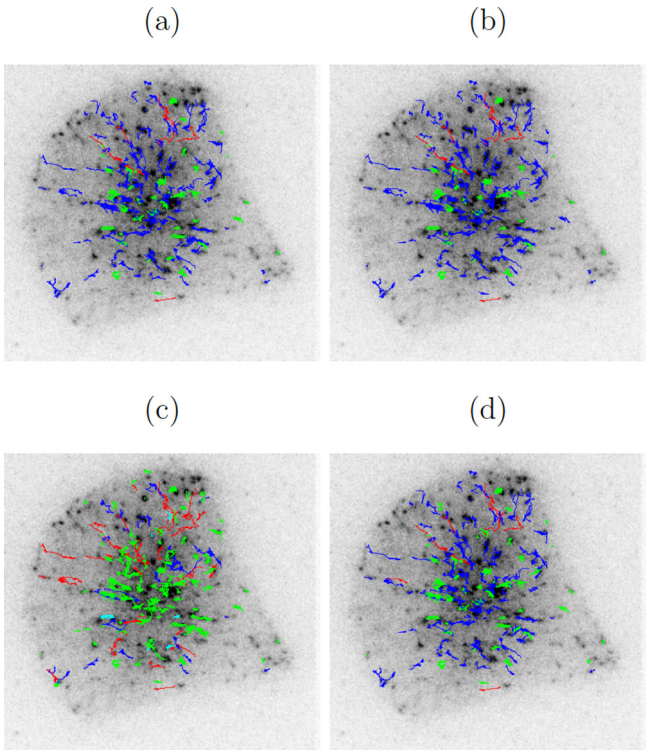

FIG. 7. Map of the classification of the trajectories of the Rab11a sequence with (a) the standard multiple-test Procedure 1, (b) the adaptive version of Procedure 1, (c) MSD, and (d) a single-test procedure. The color code is blue for Brownian motion, red for superdiffusion, green for subdiffusion, and cyan for immobile particles (for the MSD method only).

the aforementioned image sequence, we end up with 166 trajectories whose median length is $n = 84.5$. Some common statistics describing quantitatively this set of 166 trajectories are given in Fig. 8, which includes histograms of the trajectories length, of the MSD exponent β, and of the diffusion coefficient, and the MSD curves. We also give the histogram of the test statistic (12) in Fig. 9.

In Fig. 7 our results show that the four procedures, i.e., adaptive Procedure 1, standard Procedure 1, our test for a single trajectory at level 5%, and the MSD method of Feder *et al.* [19], do not produce similar classification results visually. From the simulations, we found that the MSD method tends to wrongly overdetect subdiffusion and superdiffusion (see Tables VI and VII). This is probably true also in the case of a real Rab11a sequence. In Table VIII we give the proportion of each type of diffusion for the different aforementioned methods.

TABLE VIII. Percentages of Brownian, superdiffusive, and subdiffusive trajectories in the Rab11a sequence according to the different methods of classification.

Method	Brownian	Subdiffusion	Superdiffusion
standard Procedure 1	80	16	4
adaptive Procedure 1	73	23	4
single test	66	28	6
MSD	16	63	21

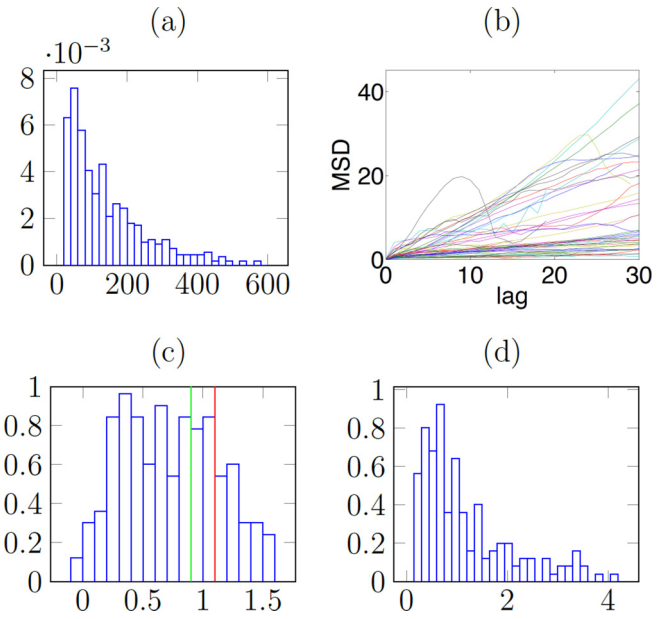

FIG. 8. Descriptive statistics of the 166 trajectories of the RAb11a sequence. (a) Histogram of the trajectories length. (b) The MSD curves of the first 50 trajectories. We plot only the first 30 points of the curves. (c) Histogram of the exponent β obtained from a linear regression of the log(MSD). The green and red vertical lines correspond to the thresholds $\beta = 0.9$ and $\beta = 1.1$, respectively, proposed by [19] for classifying the trajectories. (d) Histogram of the diffusion coefficient (in $\mu m^2\, s^{-1}$) estimated with the estimator (19) which corresponds to the first point of the MSD curve.

The adaptive Procedure 1 tends to decrease the number of Brownian trajectories compared to the standard Procedure 1. It is not surprising as the adaptive Procedure 1 is defined to be more powerful than the standard Procedure 1: It more easily rejects the null hypothesis. This gain in power benefits the alternative H_1 (subdiffusion). In fact, we detect 23% of subdiffusion for the adaptive Procedure 1 against 16% for the standard Procedure 1 while both detect 4% of superdiffusion

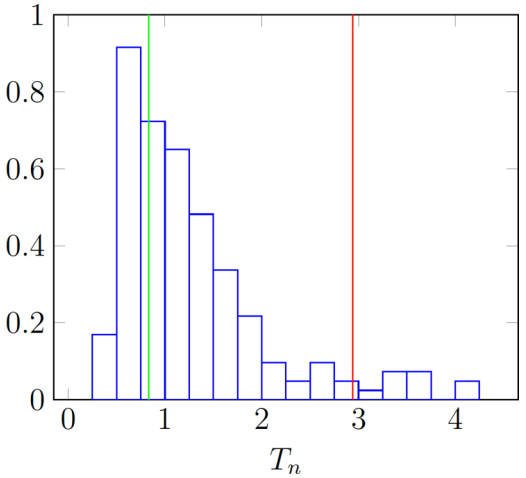

FIG. 9. Histogram of the test statistic T_n obtained from the Rab11a sequence. The green (red) vertical line represents the quantile of order 2.5% (97.5%) of the asymptotic distribution of T_n.

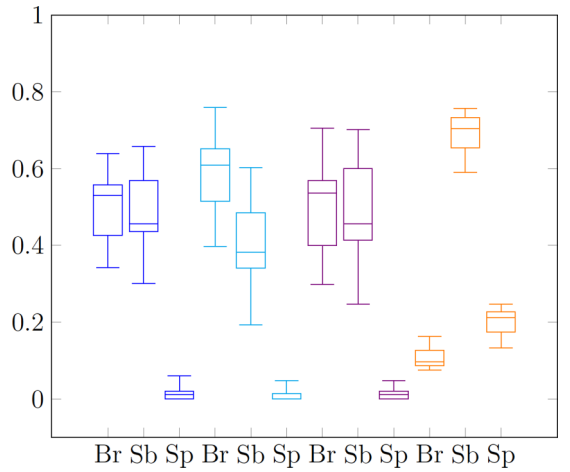

FIG. 10. Box plots of the proportions of Brownian motion, subdiffusion, and superdiffusion computed from 12 Rab11a sequences obtained with the single-test procedure (blue), Procedure 1 (cyan), the adaptive Procedure 1 (violet), and the MSD method (orange). Here Br stands for Brownian motion, Sb for subdiffusion, and Sp for superdiffusion.

(see Table VIII). The single-test procedure detects even less Brownian motion but we know that it cannot control the FDR. In Fig. 7 the subdiffusion trajectories labeled with the test approach are located more in the center of the cell in a region corresponding to the endosomal recycling compartment which is known to organize Rab11a carrier vesicles [29]. It is also true for the subdiffusion trajectories labeled with the MSD analysis, but we have just said that there is probably an overdetection of the subdiffusion with this method. We note that we carry the classification of trajectories with our different test procedures and the MSD method on multiple sequences of Rab11a protein (see Fig. 10).

VI. SPECIFIC PROBLEMS DUE TO THE IMAGING PROCESS

In this section we discuss two problems encountered in microscopy data, namely, missing points and localization uncertainty. First, until now, we assumed that the positions of a particle $X_{t_0}, X_{t_1}, \ldots, X_{t_n}$ were observed at equispaced times, that is, $t_{i+1} - t_i = \Delta$. However, we can have missing points along the trajectory when we lose the trace of the particle over a few steps of time until the particle reappears. In the presence of missing points, we have to modify the estimator $\hat{\sigma}_n$ of σ involved in the computation of the test statistic (12). For the sake of simplicity, let suppose that we estimate σ with an estimator similar to $\hat{\sigma}_{1,n}$ [Eq. (19)] based on the first-order differences $X_{t_j} - X_{t_{j-1}}$. We propose the following estimator:

$$\hat{\sigma}^2_{1,n,\text{miss}} = \frac{1}{2\Delta I} \sum_{j=1}^{n} \left\| X_{t_j} - X_{t_{j-1}} \right\|_2^2 \mathbf{1}(t_j - t_{j-1} = \Delta), \quad (27)$$

where $\mathbf{1}(A)$ is the indicator function of event A and $I = \sum_{j=1}^{n} \mathbf{1}(t_j - t_{j-1} = \Delta)$ is the number of pairs of successive positions $(X_{t_{j-1}}, X_{t_j})$ separated by the lag time Δ. In other words, we only use the increments $X_{t_j} - X_{t_{j-1}}$ such that $t_j - t_{j-1} = \Delta$ for estimating σ. Clearly, the estimator $\hat{\sigma}_{1,n,\text{miss}}$

TABLE IX. Type I error of the single-test procedure at level $\alpha = 5\%$ depending on the number of missing points. We also give in which direction (subdiffusion H_1 or superdiffusion H_2) we make the error. We compute these type I errors of the test over 10 001 Brownian trajectories of size $n = 30$ with $\sigma = 1$ and $\Delta = 1$.

% of missing points	Direction of the error		Type I error
	H_1	H_2	
0	2.50	2.69	5.19
20	2.99	2.58	5.57
40	3.78	2.53	6.31

shares the same statistical properties as the estimator $\hat{\sigma}_{1,n}$ used where there is no missing point. Then we compute T_n with the estimator $\hat{\sigma}^2_{1,n,\text{miss}}$ and use the quantiles $q_n(\alpha/2)$ and $q_n(1-\alpha/2)$ for the single-test procedure, where n is the total number of points including the missing points. Alternatively, we can use a multiple-test procedure through the calculus of the p values $p_{1,n}$, $p_{2,n}$, and p_n, where n is again the total number of points including the missing points. We study the robustness of our single-test procedure against the presence of missing points with Monte Carlo simulations. To simulate a trajectory of total size n with missing points, we first simulate a trajectory of size n with a step of time Δ. Then we select randomly, with a discrete uniform distribution, the points to remove. We never remove the two first and two last points. We show that, even with a high proportion of missing points, our single-test procedure almost controls the type I error at a level of 5% (see Table IX). We can also see that we make more type I errors in favor of subdiffusion (hypothesis H_1) than in favor of superdiffusion (hypothesis H_2). In other words, the higher the number of missing points, the more we mix up a true Brownian trajectory with a subdiffusion. Power results similar to those given in Fig. 3 are given in Fig. 11. The power curves corresponding to different proportions of missing points (0%, 20%, and 40%) are almost the same, demonstrating the robustness of our single-test procedure against the presence of missing points.

Secondly, the measured positions X_{t_i} are different from the true positions denoted by $\tilde{X}_{t_i}$. Two factors contribute to the differences between measured and true positions: the measurement noise and the motion blurring due to the camera integration times [57]. The measurement noise is due to the fact that we observe a diffraction spot and not a single position in the image. This spot is modeled by the point spread function (PSF) of the microscope. A typical choice for the PSF is a Gaussian of variance σ_0^2 whose mean is the center of the diffraction spot. The value of σ_0^2 depends on, among other factors, the number of photons recorded in the diffraction spot: It decreases with the number of photons. For simplicity, we will not consider the problem of motion blurring. Then, with no motion blurring and a Gaussian PSF, we have

$$X_{t_i} = \tilde{X}_{t_i} + \epsilon_{t_i}, \tag{28}$$

where ϵ_{t_i} is a Gaussian white noise of variance σ_0^2. Vestergaard *et al.* [58] define the signal-to-noise ratio (SNR)

$$\text{SNR} = \frac{\sigma\sqrt{\Delta}}{\sigma_0}, \tag{29}$$

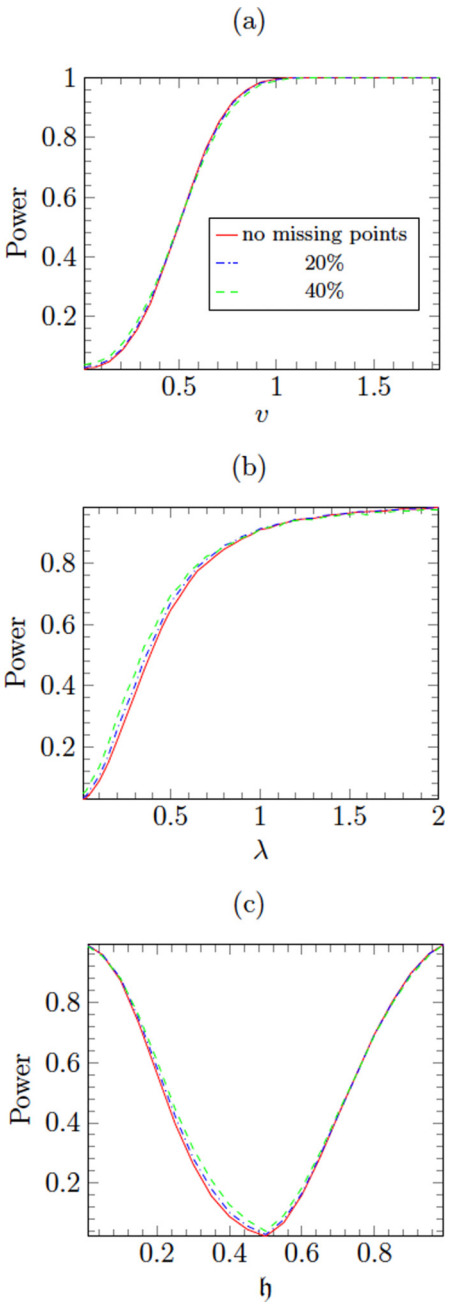

FIG. 11. Monte Carlo estimate of the power of the test at level $\alpha = 0.05$ for different percentages of missing points (0, 20%, and 40%) along trajectories of size $n = 30$. We give the power of the test for different parametric alternative hypotheses: (a) Brownian motion with drift [with the parameter $v = (v_1, v_2)$ such that $v_1 = v_2$], (b) the Ornstein-Uhlenbeck process (parameter λ), and (c) fractional Brownian motion (parameter $\mathfrak{h}$). We use 10 001 Monte Carlo replications to compute each point of the power curves. We note that we limit the study to a proportion of missing points less than 50%. Beyond 50%, we can consider that the time resolution between two observations Δ has changed. Consequently, it is no longer a problem of missing points and we can restrict our study to the case where there is less than 50% missing points.

where as before σ is the diffusion coefficient, Δ the resolution time, and σ_0 the standard deviation of the Gaussian measurement noise. We study the situation where SNR > 1, that is,

TABLE X. Type I error of the single-test procedure at level $\alpha = 5\%$ depending on the level of measurement noise. We also give in which direction (subdiffusion H_1 or superdiffusion H_2) we make the error. We compute these type I errors of the test over 10 001 Brownian trajectories.

	Direction of the error		
SNR	H_1	H_2	Type I error
1	23.15	0	23.15
2	7.46	0.42	7.88
3	4.59	1.17	5.76
∞	2.50	2.69	5.19

when the diffusive motion dominates the measurement noise. The greater the SNR, the less the trajectory is corrupted by measurement noise and, consequently, the closer the observed and true positions are. We assess the robustness of our single-test procedure against measurement noise on Monte Carlo simulations. For a given type of stochastic process, we simulate trajectories of size $n = 30$ with $\Delta = 1$ and $\sigma = 1$. We add a Gaussian noise of variance σ_0^2 according to Eq. (28). We choose a different variance σ_0 to have a different SNR [see Eq. (29)]. Table X shows the type I error rate according to different SNRs. We mainly mix real Brownian trajectories with subdiffusions for low SNR (23.15% of Brownian trajectories declared subdiffusive for SNR $= 1$). The test procedure almost controls the type I error at level α for SNR $\geqslant 3$ (see Table X). Power results similar to those given in Fig. 3 are given in Fig. 12. For subdiffusion, the power curves corresponding to low SNR are above the power curves with a high SNR [see Fig. 12(b) and the left part of Fig. 12(c)]. This means that a high amount of noise helps the detection of subdiffusion. We observe the exact opposite situation for the superdiffusion power curves [see Fig. 12(a) and the right part of Fig. 12(c)]. Actually, the noise makes the trajectories more tortuous. Hence it favors the detection of subdiffusion characterized by zigzag paths over superdiffusion characterized by straight trajectories. In all cases, the power curves corresponding to different SNRs are close (except for SNR $= 1$, a situation where the noise blurs very much the true motion), demonstrating the robustness of our procedure against a reasonable amount of noise.

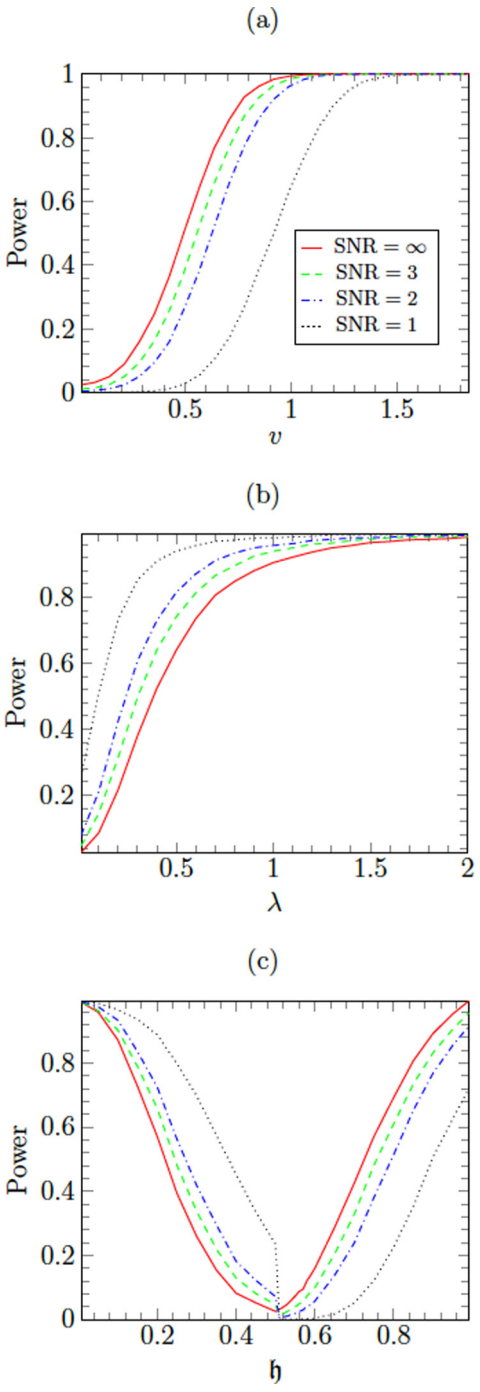

FIG. 12. Monte Carlo estimate of the power of the test at level $\alpha = 0.05$ for trajectories of size $n = 30$ according to the signal-to-noise ratio and the parameter associated with the following parametric alternatives: (a) Brownian motion with drift [with the parameter $v = (v_1, v_2)$ such that $v_1 = v_2$], (b) the Ornstein-Uhlenbeck process (parameter λ), and (c) fractional Brownian motion (parameter $\mathfrak{h}$). We use 10 001 Monte Carlo replications to compute each point of the power curves.

VII. DISCUSSION

In this paper we proposed a method for classifying the particle trajectories observed in living cells into three types of diffusion: Brownian motion, subdiffusion, and superdiffusion. We used a test approach with the Brownian motion as the null hypothesis. More specifically, we developed a nonparametric three-decision test whose alternatives are subdiffusion and superdiffusion. On the one hand, we built a single-test procedure for testing a single trajectory; on the other hand, we proposed a multiple-test procedure for testing a collection of trajectories. These procedures control, respectively, the type I error and the false discovery rate at level α. It is worth noting that the length of the trajectory n is taken into account in our classification rule. Our approach can be considered as an alternative to the MSD method. It gives more reliable results as confirmed by our Monte Carlo simulations and evaluations on real sequences of images depicting protein dynamics acquired with TIRF or single-particle tracking photoactivated localization microscopy. Other real data of interest should be

considered. Seisenberger *et al.* [59] study the infectious entry pathway of single virus particles in living cells. The study of the virus trajectory allows one to determinate by which biological process the virus reaches the nucleus to replicate. With this purpose, Seisenberger *et al.* [59] classified the trajectories due to the β exponent obtained from the MSD curves using the method of Feder *et al.* [19]. Then it will be of great interest to study these data with our method and compare the results of the two approaches. A MATLAB package of the method is available in [60].

ACKNOWLEDGMENTS

We thank Jean Salamero (UMR 144 CNRS-Institut Curie) who provided the microscopy image sequences, and for his helpful insights and assistance with experiments. Funding was provided by both Inria Rennes and CREST-Ensai-Université Bretagne Loire. This work was also supported by the French National Research Agency (France-BioImaging infrastructure–ANR-10-INBS-04).

APPENDIX A: PROOFS

1. Proof of Theorem 1

Proof of Theorem 1. Under the null hypothesis, $X_t/\sigma = B_t$ is a standard Brownian motion. Let us introduce the random variable

$$\tilde{T}_n = \max_{k=1,\dots,n} \left\| \frac{1}{\sqrt{n}} R_k \right\|_2, \tag{A1}$$

where $R_k = \sum_{j=1}^{k} (B_{j\Delta} - B_{(j-1)\Delta})/\sqrt{\Delta}$. Since $\hat{\sigma}_n$ is a consistent estimator of σ and using the Slutsky lemma, it remains to prove that $\tilde{T}_n$ converges in distribution to S_0. Using the fact that the increments of the Brownian process are independent and Gaussian, R_k is the sum of j independent identically $\mathcal{N}(0,1)$-distributed random variables. We define the process

$$W_t^{(n)} = \frac{1}{\sqrt{n}} R_{\lfloor nt \rfloor}, \quad t \in [0,1],$$

where $\lfloor x \rfloor$ denotes the integer part of $x \in \mathbb{R}$. Then we get

$$\tilde{T}_n = \sup_{t\in[0,1]} \left\| W_t^{(n)} \right\|_2. \tag{A2}$$

Due to Donsker's theorem [61], $W_t^{(n)}$ converges in distribution to the Wiener measure as $n \to \infty$ over the space of a continuous function on [0,1]. Since $x \to \sup_{t\in[0,1]} \|x(t)\|$ is a continuous function on the space of continuous functions from [0,1] to $\mathbb{R}$, $\tilde{T}_n$ converges in distribution to S_0. ■

2. Proof of Proposition 1: Convergence of the estimator (19) of the diffusion coefficient

Note that $\hat{\sigma}_n = \hat{\sigma}_{1,n}$ is strongly consistent under the null hypothesis due to the strong law of large numbers and the independence of the increments of the Brownian motion.

We focus now on the three alternatives. According to the alternative, we denote by $\mathbb{E}$ the expectation associated with the measure P of the solution of the related SDE [(8), (6), or (10)].

Proof of Brownian motion with drift. We may rewrite the strong solution of the SDE (10) as

$$X_{t_k} = X_{t_{k-1}} + v\Delta + \sigma\sqrt{\Delta}\epsilon_k, \quad k = 1,\dots,n,$$

where $\sqrt{\Delta}\epsilon_k = B_{t_k} - B_{t_{k-1}}$ and B_t is a standard Brownian motion. Then the random variables $Z_k = \|v\Delta + \sigma\sqrt{\Delta}\epsilon_k\|^2$, $k = 1\dots n$, are positive independent and identically distributed random variables and admit a moment of order 1,

$$\mathbb{E}(Z_k) = \Delta^2\|v\|^2 + 2\Delta\sigma^2.$$

Then, according to the strong law of large numbers, $\hat{\sigma}_n$ converges almost surely to $\Delta\|v\|^2/2 + \sigma^2$. ■

Proof of the Ornstein-Uhlenbeck process. Let X_t be an Ornstein-Uhlenbeck process (6). The SDE (6) admits a unique solution (see [1], Sec. 2.2.3)

$$X_t - X_s = (X_s - \theta)(e^{-\lambda(t-s)} - 1) + \sigma \int_s^t e^{-\lambda(t-u)} dB_u^{1/2}. \tag{A3}$$

Then X_t is a stationary Gaussian process where the transition density $p(s,x,t,y)$ is the density of

$$\mathcal{N}(x + (x-\theta)(e^{-\lambda(t-s)} - 1), \sigma^2(1 - e^{-2\lambda(t-s)})/2\lambda\mathbf{I}_2).$$

Then we get that

$$\begin{aligned}
&\mathbb{E}(\|X_{t+\Delta} - X_t\|^2 \mid X_t = x) \\
&= \int \|x - y\|^2 p(t,x,t+\Delta,y) dy \\
&= \|x-\theta\|^2(e^{-\lambda\Delta} - 1)^2 + \sigma^2(1 - e^{-2\lambda\Delta})/\lambda.
\end{aligned}$$

Moreover, the density μ of the stationary distribution of X_t is the Gaussian variable $\mathcal{N}(\theta, (\sigma^2\mathbf{I}_d)/2\lambda)$. Then we obtain that

$$\begin{aligned}
\mathbb{E}(\|X_{t+\Delta} - X_t\|^2) &= \int \mathbb{E}(\|X_{t+\Delta} - X_t\|^2 \mid X_t = x)\mu(x)dx \\
&= \sigma^2(e^{-\lambda\Delta} - 1)^2/\lambda + \sigma^2(1 - e^{-2\lambda\Delta})/\lambda \\
&= 2\sigma^2(1 - e^{-\lambda\Delta})/\lambda.
\end{aligned}$$

Now, according to Bibby and Sørensen (see [62], Lemma 3.1), if X_t is a stationary diffusion, $\hat{\sigma}_n^2$ converges in probability to $\mathbb{E}(\|X_{t+\Delta} - X_t\|^2)/2\Delta$. We deduce the result. ■

Proof of fractional Brownian motion. Let X_t be a fractional Brownian motion (8). Due to the self-similarity property and the stationary increments of the fractional Brownian motion, the process

$$W_t^{(n)} = \frac{X_{t_0+n\Delta t} - X_{t_0}}{(n\Delta)^{\mathfrak{h}}\sigma}, \quad t \in [0,1],$$

is a standard fractional Brownian motion. The statistic associated with the quadratic variation of the process $W_t^{(n)}$ may be defined as

$$\begin{aligned}
V_n &= \frac{1}{n}\sum_{i=1}^{n} \frac{\left\| W_{i/n}^{(n)} - W_{(i-1)/n}^{(n)} \right\|^2}{\mathbb{E}\left\| W_{i/n}^{(n)} - W_{(i-1)/n}^{(n)} \right\|^2} - 1 \\
&= \frac{\hat{\sigma}_n^2}{\sigma^2\Delta^{2\mathfrak{h}-1}} - 1.
\end{aligned}$$

According to Coeurjolly (see [63], Proposition 1), V_n converges almost surely to 0. Then we deduce that $\hat{\sigma}_n^2/\sigma^2$ tends to $\Delta^{2\mathfrak{h}-1}$ almost surely. ■

3. Proof of Proposition 2: Asymptotic behavior of the test statistic under parametric alternatives

Since the diffusion parameter σ is unknown, the test statistic (12) is normalized by an estimator of σ. Proposition 1 states that $\hat{\sigma}_n/\sigma$ converges in probability to a constant. Therefore, it is sufficient to study the asymptotic behavior of the test statistic as if σ was known. Then, in this section, we consider the test statistic T_n as

$$T_n = \frac{\max_{i=1,\dots,n} \left\| X_{t_i} - X_{t_0} \right\|_2}{\sigma \sqrt{t_n - t_0}}. \tag{A4}$$

Proof of Brownian motion with drift (H_2). The process X_t is a Brownian motion with drift (10) and may be rewritten as

$$X_{t_n} - X_{t_0} = v(t_n - t_0) + \sigma(B_{t_n} - B_{t_0}).$$

Using that B_t is a Brownian motion, the distribution of $B_{t_n} - B_{t_0}$ is $\mathcal{N}(\mathbf{0}_2, (t_n - t_0)\mathbf{I}_2)$. Then we have

$$\mathbb{E}\left(\left\| \frac{X_{t_n} - X_{t_0}}{\sigma(t_n - t_0)} - \frac{v}{\sigma} \right\|^2 \right) = \frac{2}{t_n - t_0}. \tag{A5}$$

As $t_n - t_0 = n\Delta$ we deduce that $V_n = (X_{t_n} - X_{t_0})/\sigma(t_n - t_0)$ converges in probability to v/σ. As the Euclidean norm is a continuous function, the variable $\|V_n\|$ converges in probability to $\|v\|/\sigma > 0$. Then $\sqrt{n\Delta} V_n$ converges in probability to $+\infty$. Since T_n is lower bounded by $\sqrt{n\Delta} V_n = \|(X_{t_n} - X_{t_0})\|/(\sigma\sqrt{t_n - t_0})$, the proof is complete. ■

Proof of the Ornstein-Uhlenbeck process (H_1). The process X_t is an Ornstein-Uhlenbeck process (6). We assume that the process is in its stationary regime, which means X_{t_0} is drawn from the stationary distribution that is $X_{t_0} \sim \mathcal{N}(\theta, \sigma^2/2\lambda \mathbf{I}_2)$. The SDE (6) admits a unique solution (see [1], Sec. 2.2.3)

$$X_t - \theta = (X_{t_0} - \theta)e^{-\lambda(t-t_0)} + \sigma \int_{t_0}^{t} e^{-\lambda(t-u)} dB_u^{1/2}. \tag{A6}$$

Then we may bound the test statistic T_n by

$$\frac{\left\| X_{t_0} - \theta \right\|}{\sigma\sqrt{n\Delta}} + \sum_{i=1}^{2} \max_{k=1,\dots,n} \frac{\left| X_{t_k}^i - \theta_i \right|}{\sigma\sqrt{n\Delta}}.$$

Since X_{t_0} is drawn from the stationary distribution, the term $\|X_{t_0} - \theta\|/\sqrt{n\Delta}$ converges in probability to zero. Now we show that the second term in this equation tends to zero in probability as well. We introduce the variables ξ_k^1 and ξ_k^2 defined as

$$\xi_k^i = \left(X_{t_k}^i - \theta_i\right)\sqrt{2\lambda}/\sigma, \quad k = 1, \dots, n,\ i = 1,2.$$

Then, for $i = 1,2$, the sequence $(\xi_k^i)_k$ is a standardized stationary normal sequence with the covariance function

$$r_k = \mathbb{E}\left(\xi_\ell^i \xi_{\ell+k}^i\right) = e^{-k\Delta}, \quad k \geqslant -\ell.$$

Let i be in $\{1,2\}$. Then $\{a_n[\max_{k=1,\dots,n}(\xi_k^i) - b_n]\}_n$ converges in distribution according to Leadbetter *et al.* [64], where $a_n = \sqrt{2\ln(n)}$ and $b_n = a_n - (2a_n)^{-1}[\ln\ln(n) + \ln(4\pi)]$. We deduce that $\max_{k=1,\dots,n}(\xi_k^i)/\sqrt{n\Delta}$ converges in probability to 0. Moreover, since $(\xi_k^i)_k$ is a centered Gaussian process, then $\max_{k=1,\dots,n}(-\xi_k^i)/\sqrt{n\Delta}$ converges in probability to 0 by symmetry. Then we conclude that $\max_{k=1,\dots,n} |X_{t_k}^i - \theta_i|/\sqrt{n\Delta}$ converges in probability to 0. ■

Proof of the fractional Brownian motion (H_1). The process X_t is a fractional Brownian motion with $\mathfrak{h} \in (0, 1/2)$. From the property of self-similarity and stationarity of increments of the fractional Brownian motion, the process

$$Z_t^{(n)} = \frac{X_{tn\Delta + t_0} - X_{t_0}}{\sigma(n\Delta)^{\mathfrak{h}}}, \quad t \in [0,1], \tag{A7}$$

is a fractional Brownian motion. We rewrite the test statistic as

$$T_n = \frac{1}{(n\Delta)^{1/2-h}} \max_{k=1,\dots,n} \left\| Z_{k/n}^{(n)} \right\|.$$

Then T_n is bounded by

$$\frac{1}{(n\Delta)^{1/2-h}} \sum_{i=1}^{2} \max_{k=1,\dots,n} \left| Z_{k/n}^{i,(n)} \right|,$$

where $Z_t^{(n)} = (Z_t^{1,(n)}, Z_t^{2,(n)})$. The process $Z^{(n)}$ has a version with a continuous path as a result of being γ Hölder continuous for any $\gamma < \mathfrak{h}$. Let $i \in \{1,2\}$ be fixed. Then the random variable $\max_{k=1,\dots,n} |Z_{k/n}^{i,(n)}|$ is bounded by

$$M_i^{(n)} = \sup_{t \in [0,1]} |Z_t^{i,(n)}|,$$

which possesses an absolutely continuous density on $\mathbb{R}_+^*$ according to Zaïdi *et al.* [65]. That means the sequence $(\max_{k=1\dots n} \|Z_{k/n}^{(n)}\|)_n$ is tight. Since $\mathfrak{h} < 1/2$, we deduce that T_n converges in probability to 0. ■

Proof of the fractional Brownian motion (H_2). The process X_t is a fractional Brownian motion with $\mathfrak{h} \in (1/2, 1)$. From the property of self-similarity we get that

$$Y_n = \frac{\left\| X_{t_n} - X_{t_0} \right\|_2^2}{\sigma^2 (t - t_0)^{2\mathfrak{h}}} \sim \chi^2(2). \tag{A8}$$

We observe that $T_n^2 \geqslant Y_n (n\Delta)^{2\mathfrak{h}-1}$. Let x be a positive constant. We have

$$\begin{aligned} P(T_n < x) &\leqslant P(Y_n (n\Delta)^{2\mathfrak{h}-1} < x^2) \\ &\leqslant P(Y_n < x^2/(n\Delta)^{2\mathfrak{h}-1}). \end{aligned} \tag{A9}$$

Since $\mathfrak{h} > 1/2$, $x^2/(n\Delta)^{2\mathfrak{h}-1}$ converges to 0 as $n \to \infty$. Then the right-hand side of (A9) converges to 0. That means $P(T_n < x)$ converges to 0 as $n \to \infty$ and T_n converges to $+\infty$ in probability. ■

4. Dependence of the power on the parameters of the parametric alternatives

Lemma 2. Let X_t be a Brownian motion with drift (10). Let $\hat{\sigma}_n$ be the estimator of the diffusion coefficient defined in Eq. (19). The distribution of T_n (12) depends only on the parameter $v\sqrt{\Delta}/\sigma$ and the trajectory size n.

Proof of Lemma 2. We may rewrite the strong solution of the SDE (10) as

$$X_{t_k} = X_{t_{k-1}} + v\Delta + \sigma\sqrt{\Delta}\epsilon_k, \quad k = 1, \dots, n,$$

where $\sqrt{\Delta}\epsilon_k = B_{t_k} - B_{t_{k-1}}$ and B_t is a standard Brownian motion. Then ϵ_k is a sequence of independent Gaussian

variables $\mathcal{N}(0,1)$. Furthermore, we have immediately

$$X_{t_k} - X_{t_0} = vk\Delta + \sigma\sqrt{\Delta}\sum_{i=1}^{k}\epsilon_i, \quad k = 1,\ldots,n.$$

Finally, the test statistic T_n may be rewritten as

$$T_n = \frac{\max_{k=1,\ldots,n}\left\| k\frac{v\sqrt{\Delta}}{\sigma} + \sum_{i=1}^{k}\epsilon_i \right\|}{\sqrt{\frac{1}{2}\sum_{i=1}^{n}\left\| \frac{v\sqrt{\Delta}}{\sigma} + \epsilon_i \right\|^2}}.$$

As the distribution of ϵ_k is free of the parameters, the distribution of T_n depends only on $v\sqrt{\Delta}/\sigma$. ■

Lemma 3. Let X_t be a fractional Brownian motion (8). Let $\hat{\sigma}_n$ be the estimator of the diffusion coefficient defined in Eq. (19). The distribution of T_n (12) depends only on the parameter $\mathfrak{h}$ and the trajectory size n.

Proof of Lemma 3. The fractional Brownian motion may be described by its incremental process [66]

$$\epsilon_k = \left(X_{t_k} - X_{t_{k-1}}\right)/\sigma\Delta^{\mathfrak{h}}, \quad k \geqslant 1, \tag{A10}$$

where ϵ_k is a fractional Gaussian noise which is a stationary standardized Gaussian process with the autocovariance function $\mathbb{E}(\epsilon_k\epsilon_{k+i}) = (1/2)(|i+1|^{2\mathfrak{h}} - 2|i|^{2\mathfrak{h}} + |i-1|^{2\mathfrak{h}})$. Finally, the test statistic T_n may be rewritten as

$$T_n = \frac{\max_{k=1,\ldots,n}\left\| \sum_{i=1}^{k}\epsilon_i \right\|}{\sqrt{\frac{1}{2}\sum_{i=1}^{n}\|\epsilon_i\|^2}}.$$

Then the distribution of T_n depends only on the trajectory size n and on $\mathfrak{h}$ through the distribution of ϵ_k. ■

APPENDIX B: CASE OF THE CONTINUOUS-TIME RANDOM WALK

In this article we assumed that the particle motion was driven by the stochastic differential equation (3). In this appendix we study the performance of our test when subdiffusion is modeled by a continuous-time random walk (CTRW), a process which is not related to the SDE (3). We want to show that our test statistic (12) is relevant for dealing with other types of motion of interest in biophysics but not necessarily defined through a SDE. We note that another difference compared to the stochastic processes studied previously is that the CTRWs of interest here are not ergodic. Consequently, for this type of process, the time-averaged MSD (2) does not converge to the true MSD value, causing some problems when inferring the motion [16]. As stated in Sec. II, a CTRW arises in the situation where the particle binds to an immobile trap for a random time until moving away and binding to another trap [35]. Then a CTRW is defined through the distribution of the waiting times $w(t)$ and the distribution of the jumps between two binding events $f(\mathbf{x})$ ($\mathbf{x} \in \mathbb{R}^2$). For simplicity, we assume here that the waiting times and the jumps are independent. Subdiffusion occurs when the second moment of f is finite and the first moment of w is infinite, that is, w is likely to generate long waiting times. In fact, in this case the MSD verifies

$$\mathrm{MSD}(t) \propto t^{\beta}, \tag{B1}$$

with $0 < \beta < 1$. In this appendix we suppose that w is a power distribution with an infinite first moment

$$w(t) = \frac{\beta}{\tau}\left(1 + \frac{t}{\tau}\right)^{-(1+\beta)}, \tag{B2}$$

with the shape parameter $0 < \beta < 1$ and scaling time τ. We choose to define f as a two-dimensional Gaussian distribution of mean $\mathbf{0}_2$ and variance $\sigma^2\mathbf{I}_2$. Note that σ^2 is expressed in $\mu\mathrm{m}^2$ as the location noise variance σ_0^2, while the diffusion coefficient in the SDE (3) is expressed in $\mu\mathrm{m}^2\,\mathrm{s}^{-1}$. With this setup, we can show, following the methodology of Klafter and Sokolov [67], that

$$\mathrm{MSD}(t) = \frac{\sigma^2}{\Gamma(1+\beta)\Gamma(1-\beta)}\frac{t^{\beta}}{\tau^{\beta}}. \tag{B3}$$

As a CTRW involves waiting times, the increments $X_{t_i} - X_{t_{i-1}}$ are equal to zero if no jump occurs in the interval $[t_i, t_{i-1}]$. Consequently, the estimator of the diffusion coefficient (19)

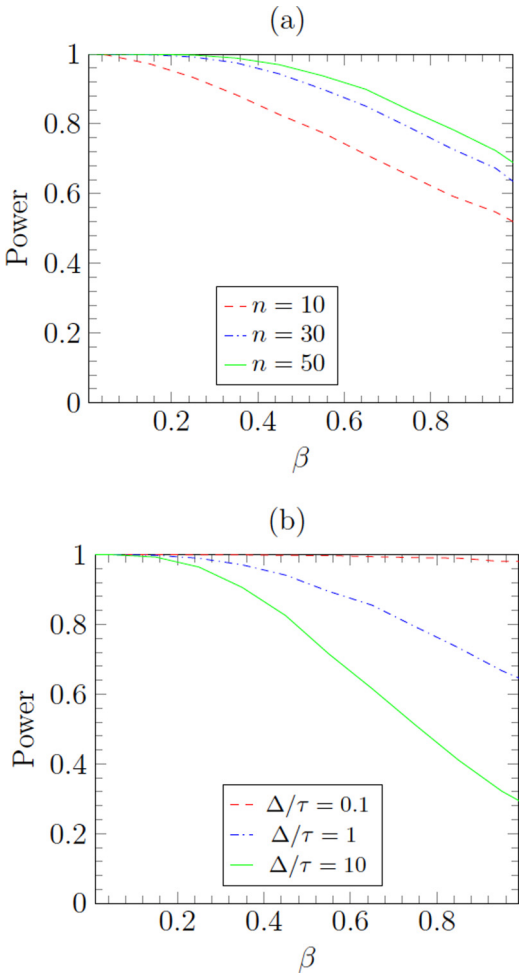

FIG. 13. Monte Carlo estimate of the power of the test at level $\alpha = 0.05$ for a CTRW with different parameters settings: (a) $\Delta/\tau = 1$ and estimated power curves for different values of n and (b) $n = 30$ and estimated power curves for different values of Δ/τ. We use 10 001 Monte Carlo replications to compute each point of the power curves.

based on the square of the increments is downward biased. Then we use instead the estimator

$$\hat{\sigma}_{1,n,\text{wait}} = \frac{1}{2\Delta J} \sum_{j=1}^{n} \left\| X_{t_j} - X_{t_{j-1}} \right\|_2^2 \mathbf{1}\left(X_{t_j} \neq X_{t_{j-1}}\right), \quad \text{(B4)}$$

where $J = \sum_{j=1}^{n} \mathbf{1}(X_{t_j} \neq X_{t_{j-1}})$ is the number of observed jumps along the trajectory. It is straightforward to show that the estimator (B4) reduces to the standard estimator (19) if the particle never stops. Then, using the estimator (B4) or (19) is equivalent for motions driven by the SDE (3) for which $P(X_{t_j} \neq X_{t_{j-1}}) = 1$. Using the estimator (B4) allows one to take into account the waiting times without interfering if no waiting times occur. We assess the performance of our single-test procedure for a CTRW with the aforementioned distributions w and f. Note that, for this form of CTRW, we can show that the power of the test only depends on the parameters n, Δ/τ, and β, with n the trajectory size and Δ the step of time as usual. Power curves are shown in Fig. 13. As expected, the lower the exponent β, the better we detect the CTRW as a subdiffusion [see Figs. 13(a) and 13(b)]. From Fig. 13(b) we can see that, for the given size $n = 30$, the power of the test is higher for low values of Δ/τ. When Δ/τ is low, the waiting times are actually long, hence the particle gets stuck for a long time at a given position and jump only a few times during the period of observation. Therefore, the test detects the CTRW as a subdiffusion with high probability [see the red dashed power curve very close to one for $\Delta/\tau = 0.1$ in Fig. 13(b)].

[1] P. C. Bressloff, *Stochastic Processes in Cell Biology* (Springer, Berlin, 2014), Vol. 41.

[2] N. Chenouard, I. Smal, F. De Chaumont, M. Maška, I. F. Sbalzarini, Y. Gong, J. Cardinale, C. Carthel, S. Coraluppi, M. Winter *et al.*, Objective comparison of particle tracking methods, Nat. Methods **11**, 281 (2014).

[3] T. Lagache, E. Dauty, and D. Holcman, Quantitative analysis of virus and plasmid trafficking in cells, Phys. Rev. E **79**, 011921 (2009).

[4] H. Qian, M. P. Sheetz, and E. L. Elson, Single particle tracking. analysis of diffusion and flow in two-dimensional systems, Biophys. J. **60**, 910 (1991).

[5] M. J. Saxton and K. Jacobson, Single-particle tracking: Applications to membrane dynamics, Annu. Rev. Biophys. Biomol. Struct. **26**, 373 (1997).

[6] S. C. Kou, Stochastic modeling in nanoscale biophysics: Subdiffusion within proteins, Ann. Appl. Stat. **2**, 501 (2008).

[7] M. Lysy, N. S. Pillai, D. B. Hill, M. G. Forest, J. W. R. Mellnik, P. A. Vasquez, and S. A. McKinley, Model comparison and assessment for single particle tracking in biological fluids, J. Am. Stat. Assoc. **111**, 1413 (2016).

[8] N. Hoze, D. Nair, E. Hosy, C. Sieben, S. Manley, A. Herrmann, J.-B. Sibarita, D. Choquet, and D. Holcman, Heterogeneity of AMPA receptor trafficking and molecular interactions revealed by superresolution analysis of live cell imaging, Proc. Natl. Acad. Sci. USA **109**, 17052 (2012).

[9] R. Metzler and J. Klafter, The random walk's guide to anomalous diffusion: A fractional dynamics approach, Phys. Rep. **339**, 1 (2000).

[10] H. Berry and H. Chaté, Anomalous diffusion due to hindering by mobile obstacles undergoing Brownian motion or Ornstein-Ulhenbeck processes, Phys. Rev. E **89**, 022708 (2014).

[11] M. J. Saxton, Anomalous diffusion due to obstacles: A Monte Carlo study, Biophys. J. **66**, 394 (1994).

[12] Y. Meroz and I. M. Sokolov, A toolbox for determining subdiffusive mechanisms, Phys. Rep. **573**, 1 (2015).

[13] Z. Schuss, *Theory and Applications of Stochastic Processes: An Analytical Approach*, Applied Mathematical Sciences (Springer, New York, 2009), Vol. 170.

[14] M. Magdziarz, A. Weron, K. Burnecki, and J. Klafter, Fractional Brownian Motion Versus the Continuous-Time Random Walk: A Simple Test for Subdiffusive Dynamics, Phys. Rev. Lett. **103**, 180602 (2009).

[15] X. Michalet, Mean square displacement analysis of single-particle trajectories with localization error: Brownian motion in an isotropic medium, Phys. Rev. E **82**, 041914 (2010).

[16] S. Burov, J.-H. Jeon, R. Metzler, and E. Barkai, Single particle tracking in systems showing anomalous diffusion: The role of weak ergodicity breaking, Phys. Chem. Chem. Phys. **13**, 1800 (2011).

[17] J.-H. Jeon, V. Tejedor, S. Burov, E. Barkai, C. Selhuber-Unkel, K. Berg-Sørensen, L. Oddershede, and R. Metzler, *In Vivo* Anomalous Diffusion and Weak Ergodicity Breaking of Lipid Granules, Phys. Rev. Lett. **106**, 048103 (2011).

[18] Y. A. Kutoyants, *Statistical Inference for Ergodic Diffusion Processes* (Springer Science+Business Media, New York, 2013).

[19] T. J. Feder, I. Brust-Mascher, J. P. Slattery, B. Baird, and W. W. Webb, Constrained diffusion or immobile fraction on cell surfaces: A new interpretation, Biophys. J. **70**, 2767 (1996).

[20] G. Didier and K. Zhang, The asymptotic distribution of the pathwise mean-square displacement in single-particle tracking experiments, J. Time Ser. Anal. **38**, 395 (2017).

[21] A. S. Pisarev, S. A. Rukolaine, A. M. Samsonov, and M. G. Samsonova, Numerical analysis of particle trajectories in living cells under uncertainty conditions, Biophysics **60**, 810 (2015).

[22] N. Monnier, S.-M. Guo, M. Mori, J. He, P. Lénárt, and M. Bathe, Bayesian approach to MSD-based analysis of particle motion in live cells, Biophys. J. **103**, 616 (2012).

[23] N. Gal, D. Lechtman-Goldstein, and D. Weihs, Particle tracking in living cells: A review of the mean square displacement method and beyond, Rheol. Acta **52**, 425 (2013).

[24] F. W. Lund, M. L. V. Jensen, T. Christensen, G. K. Nielsen, C. W. Heegaard, and D. Wüstner, Spattrack: An imaging toolbox for analysis of vesicle motility and distribution in living cells, Traffic **15**, 1406 (2014).

[25] M. J. Saxton, Lateral diffusion in an archipelago. Single-particle diffusion, Biophys. J. **64**, 1766 (1993).

[26] T. Wagner, A. Kroll, C. R. Haramagatti, H.-G. Lipinski, and M. Wiemann, Classification and segmentation of nanoparticle diffusion trajectories in cellular micro environments, PLoS ONE **12**, e0170165 (2017).

[27] J. P. Shaffer, Control of directional errors with stagewise multiple test procedures, Ann. Stat. **8**, 1342 (1980).

[28] Y. Benjamini and Y. Hochberg, On the adaptive control of the false discovery rate in multiple testing with independent statistics, J. Educ. Behav. Stat. **25**, 60 (2000).

[29] J. C. Schafer, N. W. Baetz, L. A. Lapierre, R. E. McRae, J. T. Roland, and J. R. Goldenring, Rab11-fip2 interaction with myo5b regulates movement of rab11a-containing recycling vesicles, Traffic **15**, 292 (2014).

[30] F. C. Klebaner, *Introduction to Stochastic Calculus with Applications* (Imperial College Press, London, 2012), Chap. 8.

[31] Y. Mishura, *Stochastic Calculus for Fractional Brownian Motion and Related Processes*, Lecture Notes in Mathematics (Springer, Berlin, 2008), Vol. 1929.

[32] D. Nualart and Y. Ouknine, Regularization of differential equations by fractional noise, Stoch. Process. Appl. **102**, 103 (2002).

[33] C. Fuchs, *Inference for Diffusion Processes: With Applications in Life Sciences* (Springer Science+Business Media, Berlin, 2013), Sec. 6.1.3.

[34] A. Einstein, *Investigations on the Theory of the Brownian Movement* (Courier, Mineola, 1956).

[35] M. J. Saxton, Anomalous diffusion due to binding: A Monte Carlo study, Biophys. J. **70**, 1250 (1996).

[36] P. C. Bressloff and J. M. Newby, Stochastic models of intracellular transport, Rev. Mod. Phys. **85**, 135 (2013).

[37] S. K. Ghosh, A. G. Cherstvy, and R. Metzler, Non-universal tracer diffusion in crowded media of non-inert obstacles, Phys. Chem. Chem. Phys. **17**, 1847 (2015).

[38] S. K Ghosh, A. G. Cherstvy, D. S. Grebenkov, and R. Metzler, Anomalous, non-Gaussian tracer diffusion in crowded two-dimensional environments, New J. Phys. **18**, 013027 (2016).

[39] P. Reimann, Brownian motors: Noisy transport far from equilibrium, Phys. Rep. **361**, 57 (2002).

[40] T. C. Elston, A macroscopic description of biomolecular transport, J. Math. Biol. **41**, 189 (2000).

[41] C. S. Peskin and G. Oster, Coordinated hydrolysis explains the mechanical behavior of kinesin, Biophys. J. **68**, 202S (1995).

[42] V. Tejedor, O. Bénichou, R. Voituriez, R. Jungmann, F. Simmel, C. Selhuber-Unkel, L. B. Oddershede, and R. Metzler, Quantitative analysis of single particle trajectories: Mean maximal excursion method, Biophys. J. **98**, 1364 (2010).

[43] D. Rasch, Hypothesis testing and the error of the third kind, Psychol. Test Assess. Model. **54**, 90 (2012).

[44] D. Florens-Zmirou, Approximate discrete-time schemes for statistics of diffusion processes, Statistics **20**, 547 (1989).

[45] G. J. Jiang and J. L. Knight, A nonparametric approach to the estimation of diffusion processes, with an application to a short-term interest rate model, Econometric Theory **13**, 615 (1997).

[46] I. V. Basawa and B. L. S. Prakasa Rao, in *Statistical Inferences for Stochastic Processes*, edited by I. V. Basawa (Academic Press, New York, 1980), Lemma 4.2.

[47] A. N. Borodin and P. Salminen, *Handbook of Brownian Motion—Facts and Formulae*, Probability and its Applications (Birkhäuser, Basel, 1996), formula 1.1.4.

[48] A. Grandhi, *Multiple Testing Procedures for Complex Structured Hypotheses and Directional Decisions* (New Jersey Institute of Technology, Newark, 2015).

[49] E. Roquain, Type I error rate control in multiple testing: A survey with proofs, J. Soc. Fr. Stat. **152**, 3 (2011).

[50] J. P. Shaffer, Multiple hypothesis testing, Annu. Rev. Psychol. **46**, 561 (1995).

[51] W. Guo and J. P. Romano, On stepwise control of directional errors under independence and some dependence, J. Stat. Plan. Infer. **163**, 21 (2015).

[52] Y. Benjamini and Y. Hochberg, Controlling the false discovery rate: A practical and powerful approach to multiple testing, J. R. Stat. Soc. B **57**, 289 (1995).

[53] H. Finner and M. Roters, On the false discovery rate and expected type I errors, Biometrical J. **43**, 985 (2001).

[54] C. Kervrann, C. O. S. Sorzano, S. T. Acton, J.-C. Olivo-Marin, and M. Unser, A guided tour of selected image processing and analysis methods for fluorescence and electron microscopy, IEEE J. Select. Top. Signal Process. **10**, 6 (2016).

[55] N. Chenouard *et al.*, Multiple hypothesis tracking for cluttered biological image sequences, IEEE Trans. Pattern Anal. Mach. Intell. **35**, 2736 (2013).

[56] http://icy.bioimageanalysis.org/

[57] A. J. Berglund, Statistics of camera-based single-particle tracking, Phys. Rev. E **82**, 011917 (2010).

[58] C. L. Vestergaard, P. C. Blainey, and H. Flyvbjerg, Optimal estimation of diffusion coefficients from single-particle trajectories, Phys. Rev. E **89**, 022726 (2014).

[59] G. Seisenberger, M. U. Ried, T. Endress, H. Büning, M. Hallek, and C. Bräuchle, Real-time single-molecule imaging of the infection pathway of an adeno-associated virus, Science **294**, 1929 (2001).

[60] http://serpico.rennes.inria.fr/doku.php?id=software:thot:index

[61] P. Billingsley, *Convergence of Probability Measures* (Wiley, New York, 2013), Theorem 8.2.

[62] B. M. Bibby and M. Sørensen, Martingale estimation functions for discretely observed diffusion processes, Bernoulli **1**, 17 (1995).

[63] J.-F. Coeurjolly, Estimating the parameters of a fractional Brownian motion by discrete variations of its sample paths, Stat. Infer. Stoch. Process. **4**, 199 (2001).

[64] M. R. Leadbetter, G. Lindgren, and H. Rootzén, *Extremes and Related Properties of Random Sequences and Processes* (Springer, Berlin, 1983), Theorem 4.3.3.

[65] N. L. Zaïdi and D. Nualart, Smoothness of the law of the supremum of the fractional Brownian motion, Electron. Commun. Probab. **8**, 102 (2003).

[66] M. S. Taqqu, in *Theory and Applications of Long-Range Dependence*, edited by P. Doukhan, G. Oppenheim, and M. S. Taqqu (Birkhäuser, Boston, 2003), p. 5.

[67] J. Klafter and I. M. Sokolov, *First Steps in Random Walks: From Tools to Applications* (Oxford University Press, Oxford, 2011), Chap. 3.